Enhancing preservation

Addressing humidity challenges in Indonesian heritage buildings through advanced detection methods point cloud data

Alkadri, Miktha Farid; Yuliana, Yuliana; Agung, Muhammad Rafif Cahyadi; Rahman, Muhammad Arif; Hein, Carola

DOI
10.1016/j.rineng.2024.103292

Publication date
2024

Document Version
Final published version

Published in
Results in Engineering

Citation (APA)
Alkadri, M. F., Yuliana, Y., Agung, M. R. C., Rahman, M. A., & Hein, C. (2024). Enhancing preservation: Addressing humidity challenges in Indonesian heritage buildings through advanced detection methods point cloud data. *Results in Engineering*, *24*, Article 103292. https://doi.org/10.1016/j.rineng.2024.103292

Results in Engineering 24 (2024) 103292

Contents lists available at ScienceDirect

Results in Engineering

journal homepage: www.sciencedirect.com/journal/results-in-engineering

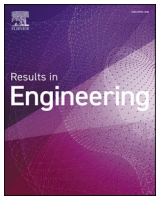

Research paper

Enhancing preservation: Addressing humidity challenges in Indonesian heritage buildings through advanced detection methods point cloud data

Miktha Farid Alkadri [a,*], Yuliana Yuliana [a], Muhammad Rafif Cahyadi Agung [b], Muhammad Arif Rahman [a], Carola Hein [c]

[a] Research Cluster of Architectural Sciences and Building Technology (ASBT), Department of Architecture, Faculty of Engineering, Universitas Indonesia, Kampus Baru Depok, West Java, 16424, Indonesia
[b] Department of Architecture and Engineering Technology (AET), Faculty of Architecture and the Built Environment, TU Delft, Jualianalaan 134, The Netherlands
[c] Department of Architecture, Faculty of Architecture and the Built Environment, TU Delft, Jualianalaan 134, The Netherlands

ARTICLE INFO

Keywords:
Cultural heritage building
3D Scanning
Thermal properties
Optical properties
Blinn–Phong BRDF

ABSTRACT

Heritage buildings are valuable assets that represent national cultural identity. Proper building maintenance is a major issue for preservation, as building monitoring aspects and preventive measures are often only taken after physical damage happens. In the context of Indonesian heritage buildings, high levels of humidity which may cause condensation and soil dampness are often overlooked. Early detection methods are urgently required to effectively detect potential risks of condensation. This study aims to investigate condensation risk for heritage building surfaces by calculating thermal properties (i.e., emissivity, albedo) and Blinn–Phong BRDF values through the integration of thermal imaging and 3D scanning techniques. This approach supports architects and conservators in making informed decisions to protect and maintain cultural heritage structures. The study also highlights gaps in current Indonesian regulations regarding moisture presence and condensation risk detection in heritage buildings.

1. Introduction

1.1. General background

Cultural heritage buildings play a vital role as national assets and emblematic embodiments of cultural identity. However, preserving cultural heritage buildings remains a great challenge, especially in humid tropical countries like Indonesia, where environmental conditions frequently precipitate physical deterioration. Elevated atmospheric moisture content is often the reason for deterioration of cultural heritage sites. The presence of moisture gradually poses a significant peril, potentially leading to complications such as condensation, high level of humidity, soil moisture, and analogous issues [1]. As per Sesana et al. [2], the incremental changes in climate conditions pose significant threats to the indoors environments of heritage structures. These threats manifest through mechanical degradation induced by phenomena like freeze-thaw cycles and salt crystallization cycles, leading to physical harm to hygroscopic materials such as wood and masonry. Additionally, there is chemical and biological deterioration affecting materials such as silk, wall decorations, furniture fabrics, and paper, primarily due to insect activity and mould. Such degradation is more pronounced in regions with warmer climates and higher humidity levels, including southern European countries, the British Isles, and Scandinavian countries. Indonesia's warm climate and relative humidity levels, provokes similar degradation. For example, the Gudang Timur Batavia, located in Central Jakarta and formerly utilized as a grain warehouse during the Dutch colonial period, is one among numerous pertinent instances illustrating building decay [3]. This deterioration stems from prolonged neglect and inadequate maintenance practices. Similarly, Toko Kompak, an old drug store which was built in 1800, is equally threatened despite its significant historical relevance to Jakarta's urban history. Currently, this building exhibits conspicuous signs of material degradation, with original components such as wood and marble walls showing pronounced fissures and undergoing material deterioration. These examples demonstrate the imperative of early detection regarding potential condensation and humidity risks, aiming not only to mitigate long-term structural repercussions but also to prevent occupant health issues associated with sick building syndrome [4].

* Corresponding author.
E-mail address: miktha@ui.ac.id (M.F. Alkadri).

https://doi.org/10.1016/j.rineng.2024.103292
Received 13 September 2024; Received in revised form 21 October 2024; Accepted 30 October 2024
Available online 8 November 2024

Moisture and condensation detection are distinct yet interrelated processes. Although both are essentials for maintaining an indoor environmental quality of the building, moisture detection focuses on quantifying the amount of moisture present in building materials or structures [5] while condensation detection primarily aims to identify condensation-prone areas based on environmental conditions [6]. Furthermore, moisture detection within buildings can be categorized into two principal methodologies: physical and chemical analysis [7]. First, *physical analysis* mainly concerns the identification of physical damage resulting from condensation occurrences. Various techniques can be used for this purpose, including Ground Penetrating Radar (GPR) for probing through the masonry ceiling [8], LoRa technology using radio signals for moisture detection in wood materials within heritage structures [9], microwave spectroscopy coupled with close-range photogrammetry utilizing clustering algorithms such as t-SNE, PCA, K-Means, and hierarchical clustering [10], and 3D laser scanning utilizing laser reflectivity [11]. Second, *chemical analysis* focuses on examining the chemical reaction of moisture in the building. This, for example, can be done through Karl Fischer method that measures the water content in a material by reacting the water with a reagent containing iodine and sulfur dioxide (Mettler [12]. Another method is gravimetric technique, as conducted by Anca-Couce et al. [13]. It aims to determine the amount of substance within a mixture. Dash et al. [14] employ a cost-effective chemosensor, designated as L, to detect water molecules in a material. However, it is essential to note that while these methods are primarily used to identify moisture content in samples, it may not directly address specific issues related to condensation detection in the building context.

Among the above-mentioned approaches in detecting moisture and condensation, this study proposes the potential application of 3D laser scanning technology as a non-destructive method. Due to advancements in laser scanning technology, it's now possible to produce reality-based datasets not only due to its exceptional quality and precision within just minutes but also its capability to encompass geometric and radiometric information of the existing context [15]. Further elaboration of this technology may provide great relevance in measuring and detecting potential degradation on the surfaces of cultural heritage buildings. For example, Rocha et al. [16] integrate 3D scanning and photogrammetry to create a Heritage Building Information Modeling (H-BIM), Alkadri et al. [17] employ attributes information of point cloud data to detect small fractures in heritage building surfaces, Lerones et al. [11] incorporate 3D scanning, thermal images, and thermos hygrometer to identify moisture detection in the building. However, most of these studies primarily take place on physical appearance of the building materials so they only focus on morphological surfaces of the building while radiometric information has yet to be fully investigated. On the other hand, the optical behavior of laser beams produced by laser scanners can be used to calculate material reflectance properties (i.e., albedo, emissivity, Bidirectional Reflectance Distribution Function (BRDF)) of the building surfaces and this calculation can potentially lead to condensation detection.

Efficient environmental control is vital for such preservation efforts. Bonora, Fabbri, and Pretelli [18] emphasize that achieving an ideal indoor microclimate in heritage buildings often requires the use of HVAC systems, which can maintain relative humidity between 20 and 40 % throughout the year. This level of humidity is crucial, as it influences the likelihood of condensation, directly affecting the condition of building materials. Similarly, a study conducted by Lucchi [19], highlights the significance of energy-efficient design in heritage buildings. It introduces a framework for evaluating energy performance tailored for air-conditioned museums in tropical regions, which are often the most common museum type in these climates. This framework includes parameters like power density and energy use intensity of HVAC systems to assess their efficiency. It also suggests strategies like using LED lighting and solar-assisted HVAC systems to reduce energy consumption while preserving indoor conditions for artefacts and visitor comfort. Integrating these indicators into heritage preservation practices may enhance the energy efficiency and sustainability objectives for air-conditioned museums.

Furthermore, this study will investigate condensation risk in heritage building surfaces by specifically calculating thermal properties and BRDF values through the integration of thermal imaging and 3D scanning techniques. The integration of its potential features may offer several contributions, as follows:

- The study introduces a novel approach for the early detection of condensation in heritage buildings by integrating 3D scanning and thermal imaging techniques. This approach facilitates non-destructive identification of potential surface degradation while enabling the calculation of thermal properties, such as emissivity, and albedo values. These parameters contribute to improving the accuracy of monitoring efforts, particularly in humid tropical climates.
- This study advances the application of radiometric data, including optical properties (i.e., BRDF) extracted from point cloud datasets to assess the surface conditions of building materials. This allows further reflectance analysis of building materials for evaluation of surface moisture and condensation. This is particularly significant, as these issues have received limited attention in the domain of heritage preservation.

The study highlights the shortcomings in current Indonesian regulations regarding moisture detection and condensation risk in heritage buildings. By identifying these gaps, it provides a foundation for improving preservation standards and informing better policy-making for safeguarding cultural heritage in humid environments.The paper is structured into five chapters. The first chapter discusses the general background of the study. This is followed by literature review that elucidates further state of the art related topics such as point cloud data, condensation, and BRDF. The second chapter describes a detailed method proposed in this study. The third chapter discusses a selected case study. Results and discussion will comprehensively be explained in chapter four. Lastly, the paper presents concluding remarks from the overarching study.

2. Literature review

This study proposes a computational method to detect condensation risks in heritage building surfaces by making use of thermal imaging and laser scanning technology. Prior to delving into specifics of the proposed method, it is pertinent to highlight three pivotal topics. For example, the potential use of point cloud data offers insights into the radiometric properties encapsulated within 3D scan datasets. It is also imperative to elucidate the phenomenon of condensation occurring on building surfaces and its intricate relationship with optical properties (i.e., albedo, emissivity, BRDF), which may significantly affect the condensation risk on the building. A detailed explanation of each topic is described below.

2.1. Point cloud data

The rapid development of 3D laser scanning technology has extended across multiple disciplines within design and engineering. However, its practical implementation in the context of architectural heritage is primarily concentrated in 3D digital reconstruction. In other words, the existing studies still predominantly take geometric properties of point clouds as a main subject of investigation. As a product of laser scanning technology, on the other hand, point cloud data has supplementary metadata that corresponds to each measurement record [20]. It consists of three coordinate position $(x_i, y_i, z_i)^T \in R$, enhanced with auxiliary attributes ($a_{j,i}$), where j ranges from 1 to m_i and i represents the number of attributes per point (P_i) [21]. Here, Otepka et al. [21] described further that each point (P_i) can be represented as a vector (x_i, y_i, z_i, α_{1i}, …,

$\alpha_{m,i})^T$, the first three components are fixed, corresponding to the point's coordinates, while the remaining components vary among different points in the cloud.

Based on the above definition, the data structure of point clouds can generally be characterized into geometric and radiometric information (22), consisting of spatial position information (XYZ) [23], color information (RGB) [24] and reflection intensity (I) [25]. This attribute information can further be used to cater different tasks such as data visualization [26] and performance analysis [27]. For example, position information can be used as an index to align and select the coordinate locations of color and intensity information within the dataset. Meanwhile, RGB color can be utilized to identify specific areas based on their distinct color properties. Kobayashi et al. [23] employed this color information by calculating hue and saturation values of road signs in Japan. Similarly, Zhan et al. [28] used colorimetric similarity and spatial proximity to conduct color-based segmentation of Chinese architecture. Reflection intensity can also be employed to investigate surface morphology of the scanned dataset as it denotes the reflectivity of surface datasets [29]. This attribute can potentially be used to explore material characteristics of surface datasets.

Recent studies have explored the utilization of point cloud data's radiometric properties, particularly reflection intensity, for environmental monitoring purposes. Reflection intensity data can be used to assess surface moisture levels, as it correlates with changes in surface properties influenced by humidity Laasch, et al., [30]. For instance, Orr, et al., [31] highlighted the role of intensity values particularly using microwave and radar in detecting moisture variations in stone walls, where higher reflectance was found to correspond with drier surfaces. Similarly, Proietti, et al., [32] demonstrated that by analyzing variations in reflection intensity over time, it is possible to monitor the progression of moisture and condensation in historic buildings, thereby identifying areas at higher risk for deterioration. These studies underscore the potential of point cloud data to enhance the understanding of humidity-related challenges in heritage structures, making it a valuable tool in the preservation of Indonesian heritage buildings, where humidity is a significant concern. Given the potential application of attribute information stored in point cloud data, this study will specifically explore the further capabilities of this attributes information (i.e., radiometric properties) in relation to condensation risk in heritage building contexts

2.2. Condensation detection

Condensation is defined as the transition of water vapor into liquid water [4]. It occurs when humid air undergoes cooling below its dew point temperature due to the relatively lower temperature of the building surface. In this regard, the dew point temperature is critical in predicting condensation onset on the building surface. This parameter can be assessed through conventional methods such as reference to a Psychrometric chart or mathematical formulation as illustrated in Eq. (1) [33]:

$$Td = \frac{B1\left[ln\left(\frac{RH}{100}\right) + \frac{A1T}{B1+T}\right]}{A1 - ln\left(\frac{RH}{100}\right) - \frac{A1T}{B1+T}} \quad (1)$$

With:

T_d = Dew point temperature (^{0}C)

B_1 = 243.04 ^{0}C (constant)

A_1 = 17.625 ^{0}C (constant)

RH = Relative Humidity (%)

T = Room temperature (^{0}C)

The occurrence of condensation within a building poses a significant risk, potentially leading to structural damage or leakage. Such condensation issues are particularly prevalent in heritage structures characterized by inadequate ventilation, compromised water piping systems, or suboptimal Heating, Ventilation, and Air Conditioning (HVAC) configurations. In response to this challenge, researchers are actively exploring innovative methodologies, with particular emphasis on heritage buildings. Brown et al. [34] employed advanced 3D scanning techniques to systematically capture and analyze the surface morphology and structural integrity of docoots (doves), pigeonhole nests dating back approximately 500 years. Additionally, Alfano et al. [35] extended their investigation on dampness assessment within cultural heritage structures. Their inquiry revealed that thermographic analysis has long served as reliable method, yielding quantitatively robust measurements sensitive to subtle humidity variations or measurements deep within walls, where microclimatic impacts (i.e., temperature, relative humidity, wind, solar radiations) are minimal. However, despite its reliability, this approach is constrained by the necessity for physical contact with the building, posing a heightened risk of structural damage. Furthermore, Muradov et al. [10] devised an assessment method utilizing microwave systems, photogrammetry, and terrestrial laser scanning (TLS) to ascertain moisture content within heritage building walls. Although this method enables microwave signals to capture temperature and moisture dataset for each surface area, its surface coverage is limited, spanning dimensions of only 220 mm x 320 m.

Since 3D scanning technology provides more accurate and wider measurement areas, this study further explores the relevant approaches and parameters specifically used to calculate condensation risks. For example, optical properties on the surface of material may indicate structural behavior and reflectance characteristics of a material and these can potentially be used to further identify the condensation properties in a building.

Given the capacity to offer precise and expansive measurement capabilities from 3D scanning technologies, this study endeavours to delve further into the methodologies and parameters pertinent to the assessment of condensation risks. Notably, the study scrutinizes optical properties exhibited on material surfaces, which may serve as indicators of structural behaviour and reflectance characteristics. These properties can potentially be used to elucidate condensation impact within a building environment, thereby enriching the repertoire of tools available for such assessments.

2.3. BRDF

In general, the optical characteristics of materials offer valuable insights into their structural composition and behavior across varying environmental contexts. In relation to condensation, there are at least three reflectance properties that require further consideration, namely albedo, emissivity, and BRDF. In this regard, albedo constitutes of the fraction of incident light reflected by a surface [36]. It plays a pivotal role in the energy dynamics of urban settings by determining the absorption percentages of solar radiation. The albedo values are usually quantified on a scale ranging from 0 to 1, with lower values indicative of greater absorption, akin to a blackbody [36]. Emissivity, on the other hand, is the measure of radiation emitted from the surface of a material [36]. It is defined as the ratio of radiated light reflected from a material to the volume emitted to a blackbody at the same temperature, wavelength, and emission direction. Materials with smooth and shiny surfaces, such as plastics, ceramics, water, and polished metals, typically exhibit high-intensity values but low emissivity levels. Although emissivity and intensity values are conceptually opposite, they both pertain to surface material properties. Consequently, emissivity values can be inferred from corrected intensity data.

Drawing on the above consideration, both albedo and emissivity concepts elucidate how light and energy interact with surfaces, focusing primarily on reflected rather than received light and energy. In order to provide a more comprehensive interpretation of reflectance properties, Nicodemus introduced the concept of BRDF in 1977, defining it as the

ratio between reflected light rays and incident radiation across a surface area [37]. BRDF accounts for the directional distribution of reflected light relative to both illumination and viewing geometries. Consequently, BRDF values offer a more nuanced characterization of surface properties. In this regard, the BRDF value is determined by two primary factors, namely radiance and irradiance [38], as can be seen in Fig. 1.

BRDF encompasses various models depending on distinct surface characteristics and material reflectance attributes. Reflectance characteristics typically fall into three categories, posing challenges in certain measurement: specular, diffuse, and ambient reflection [38,39]. Specular reflection entails mirror-like light emanating from a surface in a singular direction, contrasting with diffuse reflection, which entails light scattered in all directions [40]. Ambient reflection, conversely, denotes the presence of ambient light within a space. Reflectance values across these categories range from 0 to 1 [40].

Due to the diversity of reflections and the heterogenous nature of materials, BRDF measurements are subject to variation across several models, including the Torrance Sparrow, Ross Thick Li Sparse Reciprocal (RTLSR), Phong, Blinn-Phong, and numerous others [41]. The Torrance Sparrow model stands out as a classic BRDF microfacet model widely employed in computer graphics applications [42]. Notably, its adaptability is a key asset, as its formulation does not conform to specific microfacet distribution and Fresnel functions, rendering it suitable for modelling both conductive and dielectric materials [43]. On the other hand, the RTLSR model accounts for surface roughness, shadows, and multiple scattering effects, enabling accurate representation of reflectance properties across diverse surfaces [39]. While RTLSR is a BRDF model typically used in TLS applications, conventional TLS methods used often fail to provide insight into surface smoothness levels. To anticipate that, the inclusion of specular reflection measurements becomes essential to consider.

Among BRDF models, one that incorporates specular reflection is the Phong BRDF, introduced by Phong [44]. The Phong BRDF characterizes surface light reflection as a blend of diffuse and specular reflection components [44]. However, the Phong BRDF only takes irradiance when determining its normal vector, which diverges from the mechanism of TLS dataset, where radiance and irradiance are typically unidirectional. To address deviation, the Blinn-Phong model alternatively provides relevant calculations that yield higher reflections aligning with the half vector h, which is parallel to the surface normal (7; 29).

Fig. 2 illustrates a comparative analysis between the Phong BRDF model and the Blinn-Phong BRDF model. Fig. 2a and b depict general representations of BRDF models, whereas Fig. 2c and d specifically showcase BRDF models employed in the context of TLS. Below is the basic equation used in referring to the basic Phong's BRDF [44] (see Eq. (2)).

$$F_r(v,r) = kd + ks(v \cdot r) \tag{2}$$

where:

F_r = BRDF Value
v = The vector of the observer's point of view
r = Radiance
kd = Diffuse coefficient
ks = Specular coefficient

The Blinn-Phong BRDF model, depicted in Fig. 2b, introduces an additional vector denoted as **H**, representing the vector between radiance and irradiance. Moreover, the angle of incidence is defined as the angle between the **H** vector and the surface normal vector. The general equation governing the Blinn-Phong model is expressed as follows [45] (see Eq.3):

$$F_r(n,h) = kd + ks(n \cdot h) \tag{3}$$

where:

F_r = BRDF Value
n = The vector of the observer's point of view
h = Vector between radiance and irradiance
kd = Diffuse coefficient
ks = Specular coefficient

Given the utilization of TLS in this study, the laser beam is both transmitted and emitted in a singular direction (see Fig. 2c& 2d). This results in vector H facing the same direction. The dot product operation

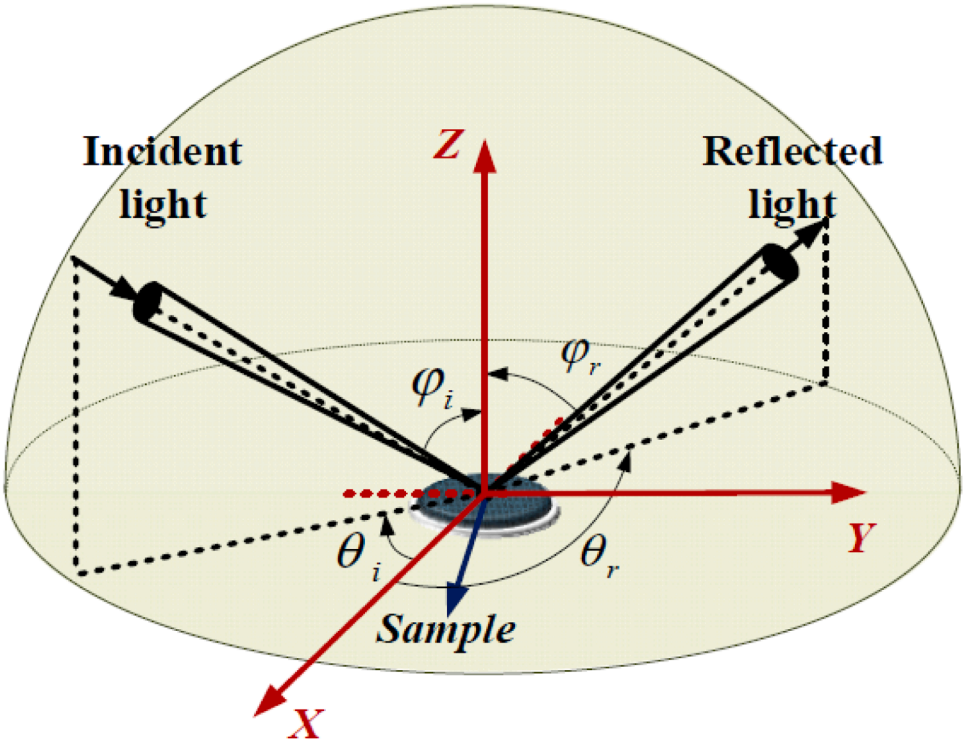

Fig. 1. Spatial distribution diagram of BRDF hemisphere [38].

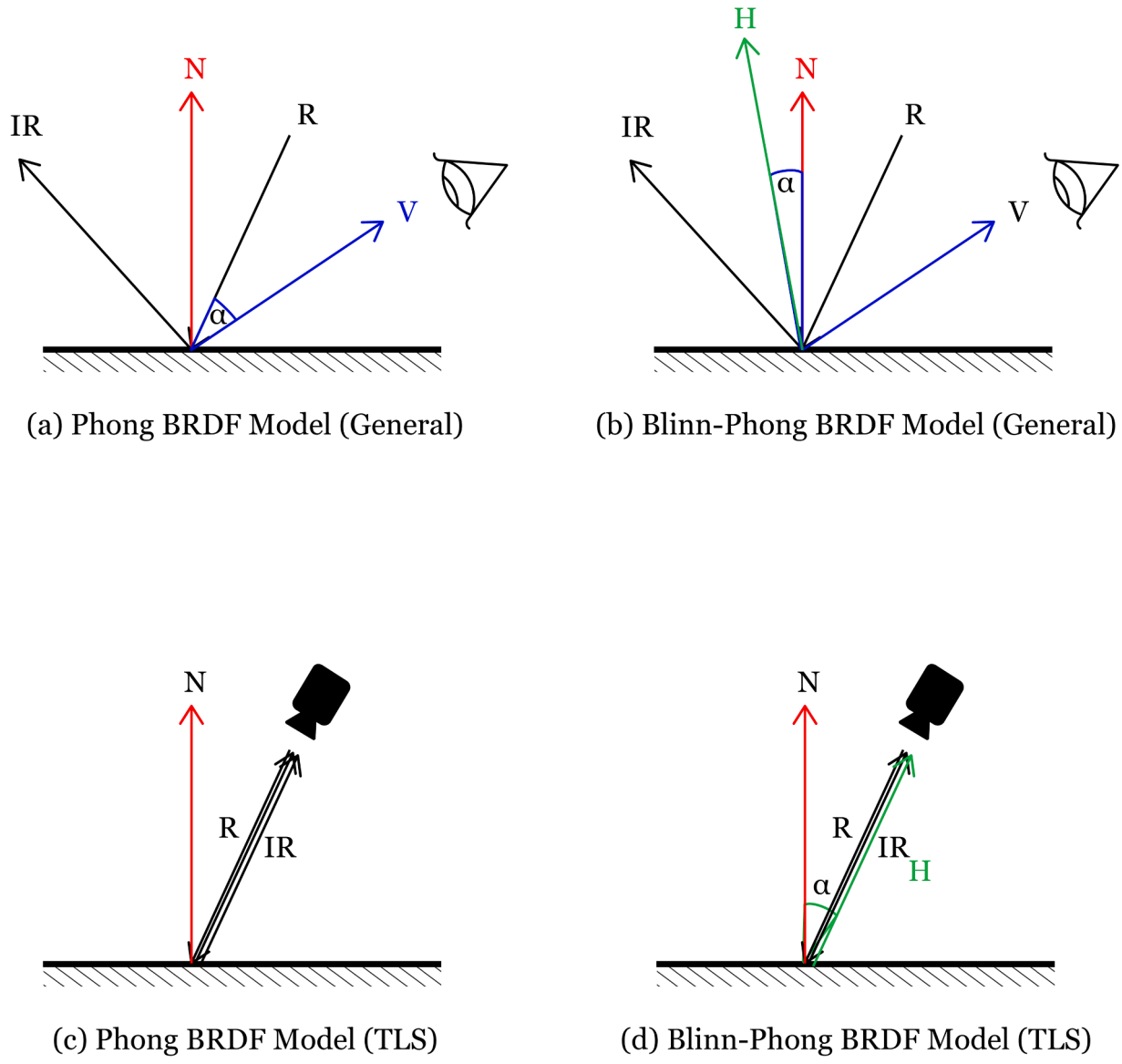

Fig. 2. The difference between Phong and Blinn-Phong BRDF in general concept and TLS (elaborated from 45).

between vector **n** and **h** is elaborated below (see Eq. 4):

$$n \cdot h = |n||h|cos\alpha,\ |n| = 1$$

$$\frac{n \cdot h}{|h|} = cos\alpha,\ |h| = 1$$

$$n{\cdot}h = cos\alpha \tag{4}$$

Because the magnitude of vectors n and h are both normalized to 1, the Blinn-Phong BRDF model (Eq. (3)) can be equivalently expressed as Eq. (5). This equation will be further used in the present study as it employs TLS dataset.

$$F_r(n,h) = kd + kscos\alpha \tag{5}$$

where:

F_r = BRDF Value
n = The vector of the observer's point of view
h = Vector between radiance and irradiance
kd = Diffuse coefficient
ks = Specular coefficient
α = angle between n and h

Further elaboration of BRDF models has been employed in several studies. For example, Lerones et al. [11] leveraged the reflectivity index introduced by Angstrom [46] to discern vegetation water content as part of heritage building assessment. Krzeslowski et al. (2012) explored a novel 3D and BRDF approach for integrated heritage digitization, highlighting the pivotal role of BRDF models for generating realistic virtual 3D representation of cultural heritage structures. Their proposed method can facilitate multidirectional data integration and it can serve as a tool to achieve accurate visualization of 3D models and enhance texture fidelity. In a similar vein, Nielsen et al. [47] conducted an investigation into the ramifications of system parameters uncertainties when integrating a data-driven BRDF reconstruction approach into the standard pipeline of a structured light scanning system. Their findings indicate that uncertainties in vertex object geometry and light source properties exert minimal influence on the reconstructed BRDFs.

Drawing upon insights from previous studies, it is evident that BRDF model necessitates adjustments tailored to the specific objectives of the analysis. In this context, BRDF is utilized to assess reflectance index using a TLS dataset, where both the source angle of incidence and normal remain consistent. Furthermore, the inherent characteristics of the Blinn-Phong BRDF model render it highly pertinent to the context of

condensation detection utilizing TLS dataset examined in this study.

3. Method

The aim of this study is to develop a computational method for identifying and calculating condensation risks within the heritage building surface by employing TLS dataset in conjunction with environmental monitoring devices. The overarching method comprises five sequential steps, as illustrated in Fig. 4.

As depicted in Fig. 3, the proposed method entails a series of dataset collections using several instruments such as thermal imaging camera, SLR camera, TLS, and data logger. Each of which caters for different tasks. For example, the thermal imaging camera (i.e., Flir One Pro) is utilized to capture thermal images and acquire temperature data for each pixel on the building surface under observation. The TLS (i.e., Leica RTC360) facilitates the generation of 3D models of existing buildings through point cloud data. Concurrently, a data logger (Hobo MX1101) is deployed to record room temperature and humidity levels for subsequent analysis. SLR cameras are also used to capture the physical condition of the room. In addition, the study also employs several digital processing tools for data manipulation and analysis. For example, Ms. Excel is used to sort the raw data from actual measurements. R studio is employed for dataset processing of point cloud attributes, surface temperature dataset and statistical analysis. Cloud Compare (CC) aids in refining geometric point cloud data and visualizing 3D models derived from point clouds. Lastly, Rhinoceros and Grasshopper are used not only for segmenting thermal images but also for extracting the geometric surface of temperature datasets. Finally, the equipment is checked for accuracy through calibration. First, the Hobo Data Logger was calibrated, and the results show that the measurement uncertainty was calculated at a 95 % confidence level with a coverage factor of 2. The calibration method used was MK-03/09, JIS Z8710 1993, and ASTM E2551-07. Second, the TLS Leica RTC360 has been audited and certified according to ISO 9001. The Calibration Certificate Blue, without measurement values, issued by the Authorized Service Center corresponds to a declaration of conformity according to ISO/IEC 17050-1.

Furthermore, detailed information regarding the activities, tools, formats, and tasks corresponding to each stage of the proposed method are comprehensively illustrated in Fig. 4. In general, the method comprises three main stages: dataset collection, performance simulation, and evaluation. Each of these stages contains sequential steps that cater for different objectives and activities as follows:

3.1. Step 1 – literature review

According to ISO 22185-1:2021, structural harm resulting from water vapor infiltration into buildings is termed moisture damage [48]. This standard delineates a classification framework for assessing the severity of moisture damage, spanning from negligible to severe. Severity categorization hinges on several factors including the extent of the affected area, the degree of structural degradation, and the consequential impairment to the functionality of affected materials or components. Haverinen et al. [49] conducted a study that devised a three-tiered grading system predicated on the severity of distinct types of damage. This system encompasses grades I to III. Grade I is designated for residences exhibiting either no moisture damage or only minor instances thereof, while grade II denotes structures manifesting discernible moisture patterns. Grade III is attributed to homes afflicted with substantial issues stemming from moisture damage.

Furthermore, this study classifies potential condensation-related moisture damage into four distinct levels: potential, low, medium, and high. This categorization is derived from multiple criteria outlined in Table 1, which include the physical condition of the room, duration of exposure, ambient air temperature, relative humidity, and the specific condition of the room. In the case of room condition, condensation is heightened in rooms lacking adequate ventilation coupled with the presence of water vapor sources. Such sources may include, but are not limited to, malfunctioning air conditioning systems or improperly installed piping within walls.

According to Table 1, the initial level of damage, termed “potential” occurs when building materials or surfaces maintain a normal appearance with the room’s relative humidity ranging from 40 to 75 %. A low

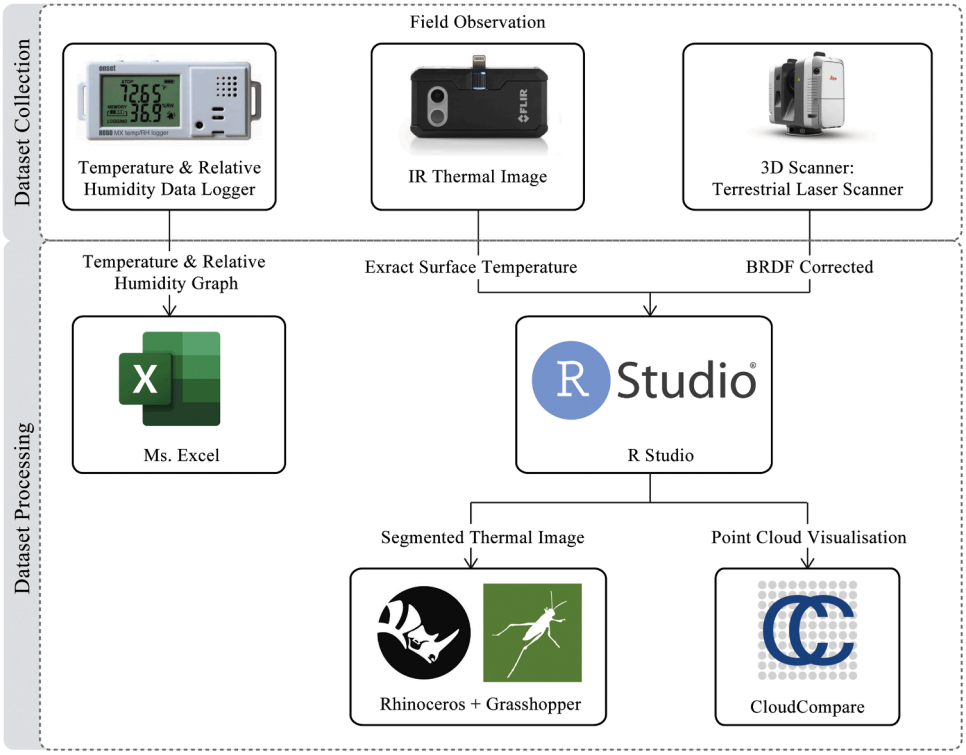

Fig. 3. Computational workflow – tools.

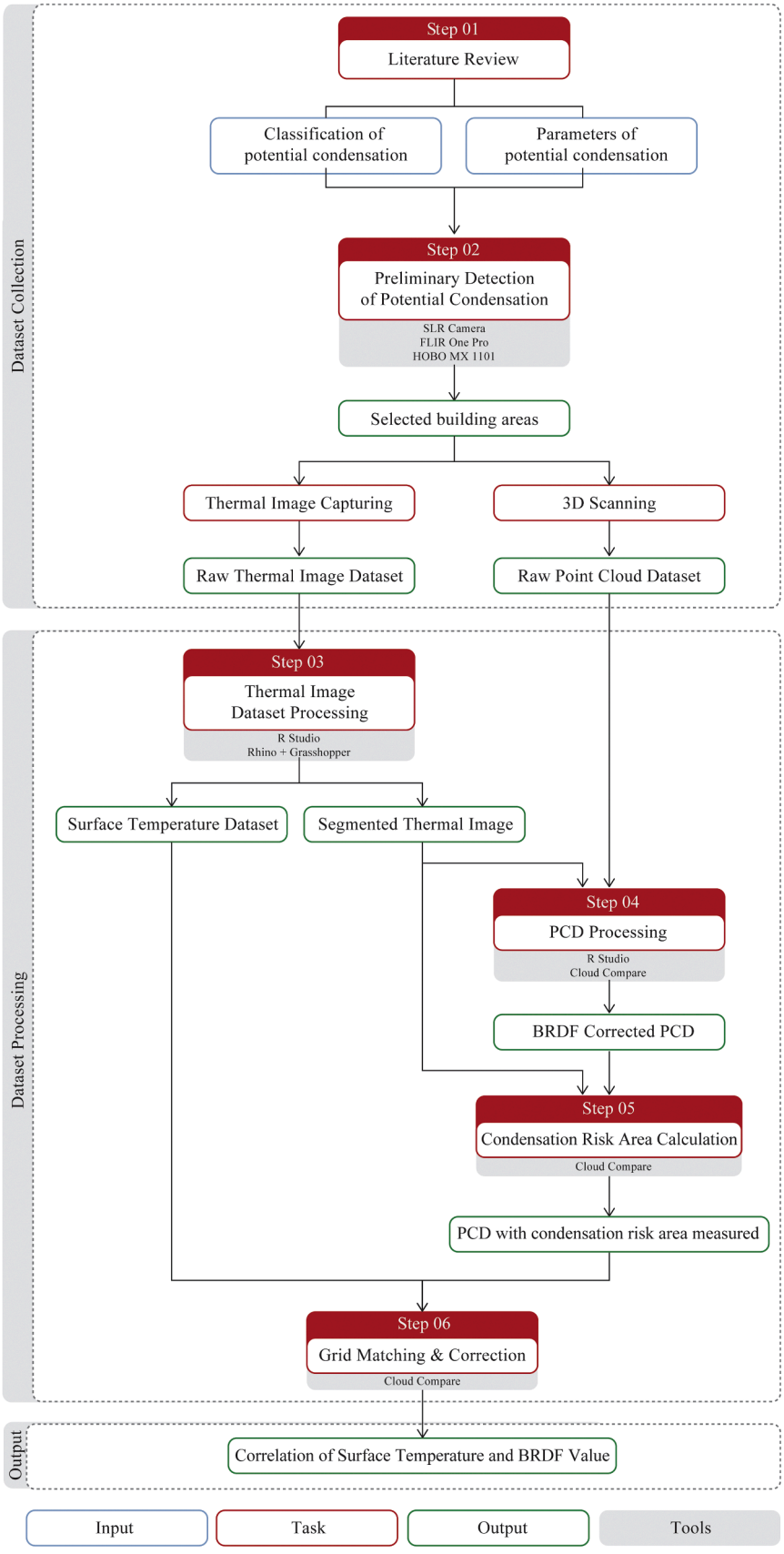

Fig. 4. Computational Workflow – Procedure.

Table 1
Four level of destruction caused by condensation.

Level of Destruction due to Condensation	Digital Image / Physical condition	Duration	Air Temperature	Relative Humidity	Room condition
Potential	Detect nothing			40 % −75 % (ASTM)	No ventilation, there are water vapour sources.
Low destruction	Dust accumulation	90 min (Li et al., 2023)	0oC-50oC	75 %−80 %	
Medium destruction	Colour change	Mould growth 24–48 h since moisture exceeded, 21 days until appear (Pasanen, 1993)	20oC-40oC	>95 %	
High destruction	Peeling paint	after years	same as above, in certain duration		

level of destruction is identified if there is an accumulation of dust in specific areas of the building, typically occurring 90 min post-condensation, with ambient air temperatures between 0 and 50 °C and relative humidity levels of 75–80 °C [4]. For a classification of medium level of destruction, a discernible color change in building materials is required, commonly resulting from mold growth that emerges 24–48 h after moisture levels exceed normal thresholds, with room temperatures of 20–40 °C and relative humidity reaching up to 95% [4]. If the condition of the room remains the same for years, this may lead to the peeling of paint on building components or materials, which is classified as a high level of destruction.

Moreover, Bonora, Fabbri, and Pretelli [18] note that achieving an ideal indoor microclimate, especially in historic buildings, often requires the use of HVAC systems. These systems help maintain relative humidity between 20 % and 40 % during both dry and wet seasons, which significantly influences material conditions and the potential for condensation. Zhang et al. [50] shared similar findings, indicating that HVAC systems, particularly those monitoring multiple parameters, are effective in assessing material conditions and the likelihood of condensation. Lerma et al. [51] confirmed that low temperatures and high relative humidity are strongly associated with a high potential for condensation, specifically at relative humidity levels of 65–67.9 % and temperatures of 15.8–16.4 °C. Furthermore, Proietti et al. [32] observed that areas with high humidity (>20 %) are more susceptible to deterioration, discoloration, and efflorescence.

3.2. Step 2 – preliminary detection of potential condensation

Fig. 5 depicts a detailed task conducted during the preliminary detection step, which involves the acquisition of pertinent environmental datasets (i.e., surface temperature, air temperature, relative humidity) conducted concurrently. In this process, digital and thermal images are superimposed to pinpoint areas exhibiting the lowest surface temperatures. Besides, a data logger is strategically placed within a designated room to record air temperature and relative humidity at five-minute intervals. This interval selection is predicated on balancing the need to gather comprehensive data without generating excessive datasets and to adequately monitor fluctuations in temperature and humidity.

In addition to environmental datasets, identification of technical issues within each room is also undertaken. This aspect is particularly critical in the context of heritage buildings, which frequently present HVAC challenges, including malfunctioning air conditioners and water leaks from damaged pipes. Both these factors are subsequently integrated to determine the condensation risk classification for each room.

3.3. Step 3 – thermal image dataset processing

This step (see Fig. 6) is essential for acquiring surface temperature data, which helps to identify areas susceptible to condensation. Following the preliminary categorization of building areas based on the destruction level, a subsequent series of images are captured using an infrared (IR) thermal camera. But this time, a more refined approach is

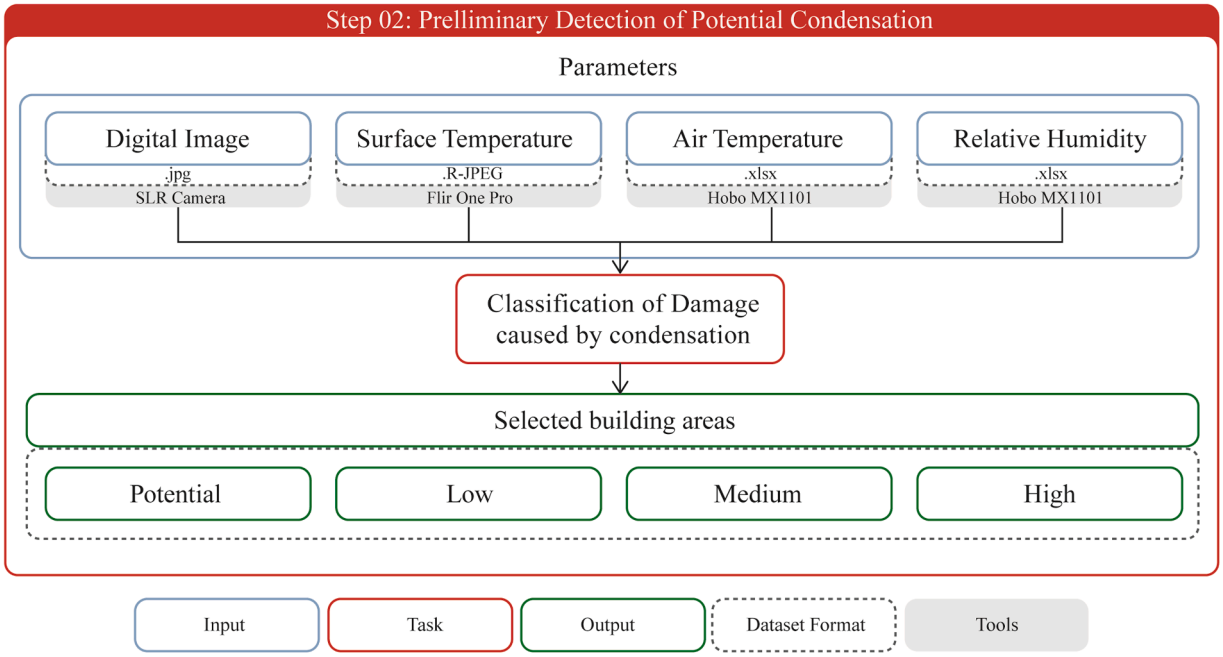

Fig. 5. Step 2: Preliminary Detection of Potential Condensation.

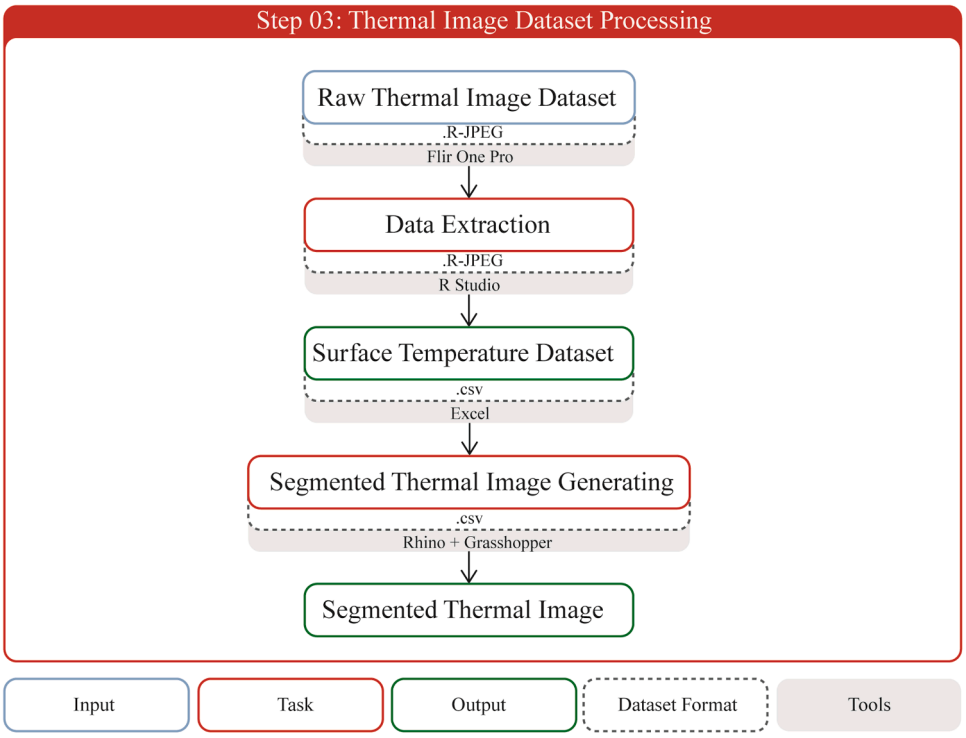

Fig. 6. Step 3: Thermal Image Dataset Processing.

used to enable investigation of specific components of the building structures such as corners and surfaces, where potential indications are most likely to occur.

This step starts with capturing the thermal images using FLIR One Pro camera with R.JPEG (radiometric JPEG) format. This format includes metadata that provides the surface temperature for each pixel within the image. The radiometric data is subsequently extracted into a .csv file format to be able to visualize in Rhino and Grasshopper tools. During visualization, the captured image undergoes segmentation into discrete pixel regions, each representing a surface temperature differential of 0.5 °C. This process refers to as image segmentation, which enables a detailed analysis of temperature variations across the imaged area.

3.4. Step 4 – point cloud dataset processing

In order to efficiently capture the entire geometry of the building, this study employs Leica RTC360 with a medium level of precision, offering an accuracy of 6 mm. As for selected areas, a high precision setting with 3 mm accuracy was utilized to ensure a more detailed dataset. In general, the raw scanning dataset contains spatial coordinates (XYZ), color information (RGB), and raw intensity values (Ir). Subsequently, raw point cloud data is registered in Leica Cyclone 360, a software to export raw dataset to e57.

The preprocessing dataset contains two parts: geometric and radiometric preprocessing (see Fig. 7). The geometric preprocessing aims to clean the dataset from outliers (unnecessary cloud of points) using outlier removal. Given the fact that point clouds often exhibit varying densities, with some regions being denser than others, a subsampling task is performed not only to eliminate excessively dense points but also to remove redundant point clouds. This process can ultimately yield a dataset with a more consistent distribution, thereby decreasing computational calculation demands at a later stage. Following geometric preprocessing, radiometric preprocessing is conducted, comprising several tasks such as computing normal, intensity corrections, and intensity normalization. In this regard, computing normal generates additional attributes known as surface normals (Nx, Ny, Nz), which represent the normal vector of each point cloud. Similarly to optics mechanism, the TLS laser beam reflects off surfaces, and the further the beam travels, the weaker the reflected signal received by the scanner. Thus, the distance between the TLS and surrounding objects can influence the signal intensity [52], necessitating correction. For intensity correction (Ic), this study utilizes Eqs. (6) (53).

$$\varepsilon = I_c = I_{raw} . \frac{1}{cos\ \alpha} \tag{6}$$

Where:
ε = emissivity
I_c = corrected intensity
I_{raw} = original intensity
α = angle of incidence

The angle of incidence represents the angle formed between the direction of the laser beam (dl) and the normal vector of the surface it reflects off (dn). This angle, denoted as α, is calculated according to Eq. (7) (53).

$$\alpha = cos^{-1}\left(\frac{\underline{dn} \cdot \underline{dl}}{|dn| \cdot |dl|}\right) \tag{7}$$

where:
α = incident angle
$\underline{dn}$ = direction of the surface normal
$\underline{dl}$ = direction of the laser pulse

Following the intensity correction, normalization is required to remap the resulting values within a range of 0 to 1. This is accomplished using the equation provided below (53):

$$I_n = \sqrt{asinh(I_c)} \tag{8}$$

where:
I_n = normalised intensity
h = Vector between radiance and irradiance
I_c = corrected intensity

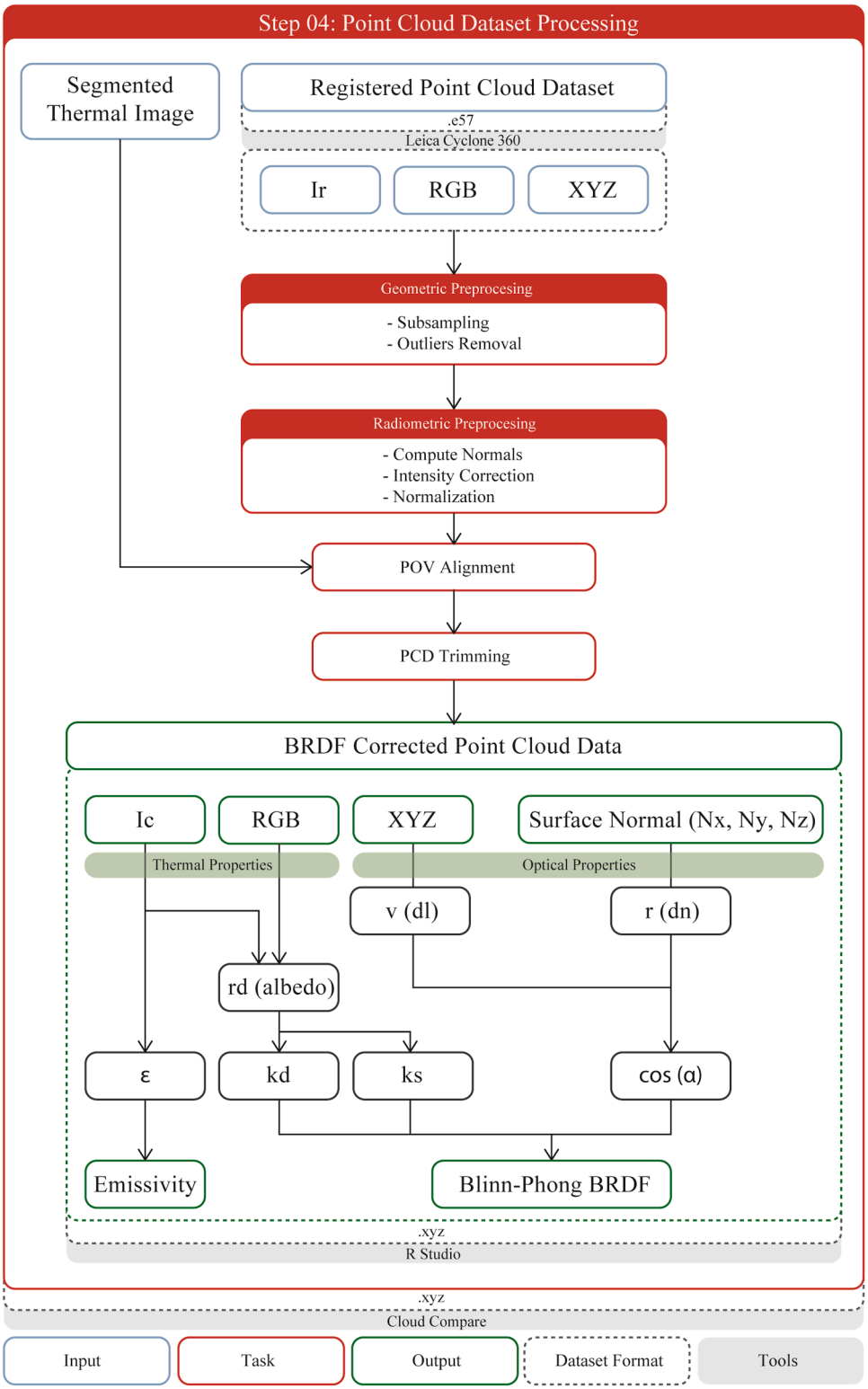

Fig. 7. Step 4: Point Cloud Dataset Processing.

Upon completing both geometric and radiometric preprocessing, the subsequent step involves aligning the point of view (POV). The resulting segmented thermal images from Step 2 are then imported into Cloud Compare, and the viewport of the point cloud is aligned to achieve the same POV. Any point clouds outside of the viewport are trimmed to match the resolution of the segmented thermal images.

Furthermore, thermal properties (i.e., albedo (rd)) within the point cloud data can be further calculated based on the corrected intensity (Ic) and RGB values. This calculation is conducted using Eq. (9) in RStudio since the diffuse coefficient (kd) is equivalent to albedo (rd) (53).

$$kd = rd = I_n . \frac{\sqrt{\frac{R^2+G^2+B^2}{3}}}{225} \tag{9}$$

where: kd = Diffuse coefficient rd = Albedo value

R = the red value
G = the green value
B = the blue value
I_c = the corrected intensity value

The diffuse and specular coefficient each range from 0 to 1. When these two coefficients are summed, their total equals 1. Thus, the equation for the specular coefficient is defined as follows:

$$ks = 1 - rd \tag{10}$$

where: ks = Specular coefficient rd = Albedo

Furthermore, the optical properties utilized in this study include the direction of the laser pulse (dl) or (v) and the direction of the surface normal (dn) or (r) to calculate the angle of incidence (α) using Eq. (7). Once the diffuse coefficient (kd), specular coefficient (ks), and angle of incidence (α) are determined, the Blinn-Phong BRDF value can be calculated using Eq. (5). This process will result in point cloud that corresponds to BRDF and emissivity value. Furthermore, this calculation was done in R-Studio. For more details on the R-Studio script, please refer to Appendix 2.

3.5. Step 5 – condensation risk mapping

In this section, the area of building components at risk for condensation will be calculated (see Fig. 8). By analyzing the selected areas segmented into different temperature ranges and comparing them with room temperature data from the HOBO data logger, the volumetric size of condensation areas can be further identified. To do so, the corrected point cloud is processed using Cloud Compare. Since the thermal images are already segmented into surface temperature data, the lowest temperature range, which is closest to the dew point temperature under current room conditions, is selected. This step will result in point cloud data with condensation risk areas.

3.6. Step 6 – grid matching

The IRT thermal imaging camera produces surface temperature for each pixel, resulting in a dataset of 307.200 temperature values for an image with a resolution of 640 x 480 pixels. In contrast, the point cloud data contains approximately 200.000 points, varying by room size. Given the significant discrepancies between surface temperature and BRDF values, an additional step is necessary to perform a correlation analysis between these two variables. This process can be seen in Fig. 9.

In order to facilitate the correlation analysis, the surface temperature dataset is firstly reduced by averaging the values for every 2 x 2 pixel cell, resulting in a down sampled dataset with a resolution of 320 x 240 pixels. Then, to match the size of the surface temperature dataset, a grid of 320 x 240 is created on the point cloud dataset for the previously measured condensation risk area. Having matched the size of datasets, the correlation analysis can be performed.

Furthermore, the process of grid matching is performed to correlate surface temperature with BRDF values. In doing so, the grid-matched cells are then sampled for comparative analysis among selected rooms. There are 40 cells extracted from the grid-matching results to ensure comparability across four rooms. The dataset is ordered based on the contrast difference between surface temperature and BRDF values, which indicates the probability of a strong correlation between the two variables. In this regard, Pearson correlation coefficient is used [11], given that both variables are continuous and exhibit a linear relationship.

4. Dataset collection

This study selected the Cut Meutia Mosque, also known as the NV De Bauploeg building (see Fig. 10), as an exploratory case for implementing the proposed method outlined in Fig. 4. The mosque is located at Taman Cut Mutiah Street, Central Jakarta, Indonesia. It was originally built in 1912 and designed by Pieter Adriaan Jacobus Moojen. Over the years, its function evolved, starting as a post office and railway office from 1942 to 1945, and as a housing consultancy and offices of religious affairs from 1964 to 1970 [54].

Following Indonesia's independence, the building was repurposed by the local community as a mosque. Significant modifications were made during this period, including the removal of the central stairs. Designed and constructed in the Art Nouveau style, the building reflects the architectural trends of its time. Currently, the Cut Meutia Mosque has been recognized as a cultural heritage site due to its European architectural style and historical significance dating back to the Dutch colonial era [55].

In general, the building of Cut Meutia Mosque is situated on a triangular site, encompassing an area of 1.792 m^2s with a circumference of 200 m [55]. The building features two entrances: the main entrance for vehicle access from the South, and an additional entrance from the

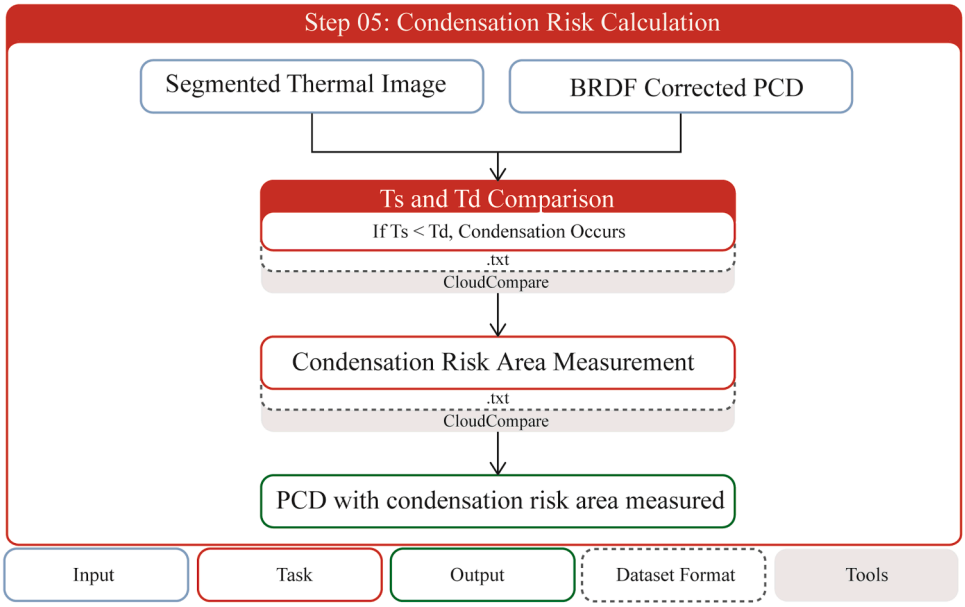

Fig. 8. Step 5: Condensation Risk Calculation.

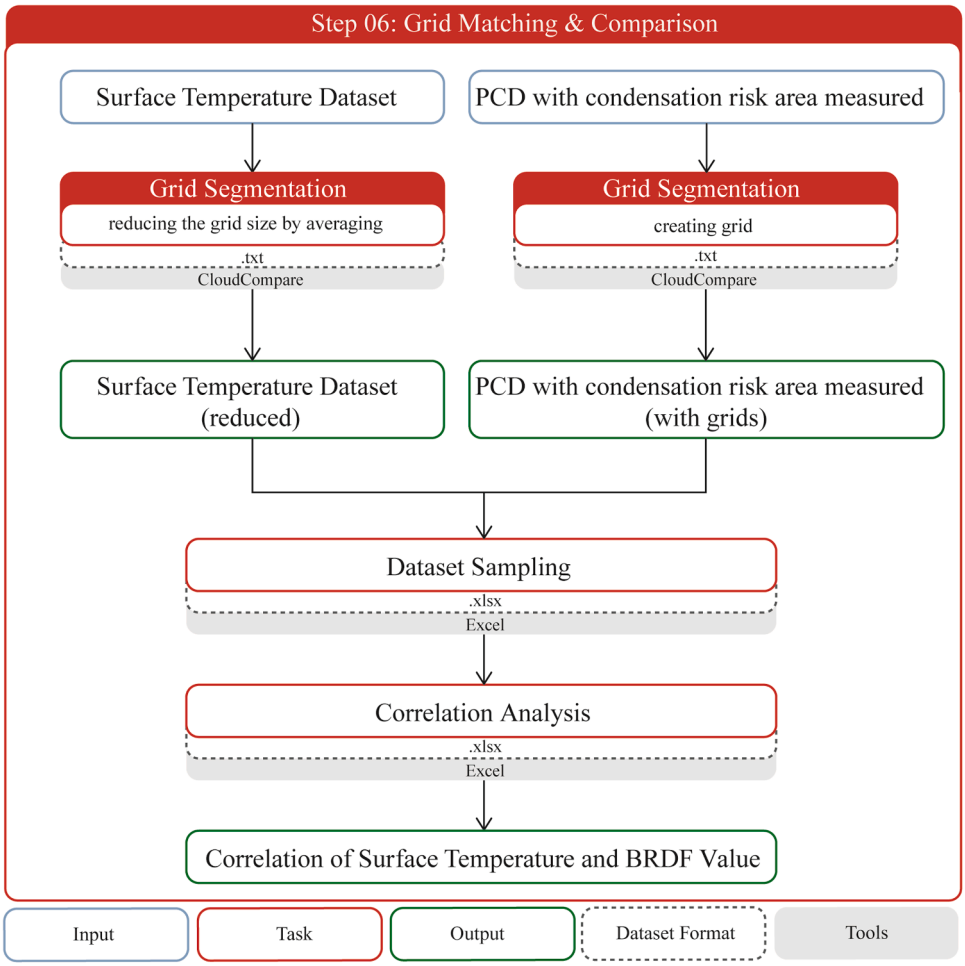

Fig. 9. Step 6: Grid Matching and Comparison.

North. The total floor area consists of 300 m^2s and a height of 22 m, the structure boasts high ceilings, despite having only two floors. The vertical distance between the first and second floors is 3.5 m, while the distance from the second floor to the roof is around 11.5 m.

Furthermore, for the purpose of this study, specific areas will be selected after conducting an environmental performance evaluation to identify rooms with a high potential for condensation.

5. Result and discussion

The present work has articulated the research into three main results, consisting of preliminary surveys, condensation risk area measurement and lastly, correlation analysis between BRDF and surface temperature. Each of which is comprehensively discussed below.

5.1. Preliminary survey of selected datasets

5.1.1. Physical observation

A detailed physical observation of the heritage building was conducted to identify potential areas at risk of condensation. Fig. 11 shows the condensation risk mapping of Cut Meutia Mosque, as a result of the physical observation. It simultaneously summarises the classification of potential condensation that may occur at the Cut Meutia Mosque. Fig. 12 depicts a preliminary mapping of condensation areas, showcasing the existing conditions and thermal images of each room in the Cut Meutia Mosque. Observation spots within each room are marked by grey and orange dots. Grey dots indicate no physical damage, while orange dots signify physical damage to building elements, such as damage components, blue or yellow stains, peeling paint, etc. Additionally, the mapping includes technical issues potentially causing condensation and dampness in building elements. According to the physical observation, there are at least 13 identified technical issues: 7 for standing air conditioners (red dots), 2 for indoor split unit air conditioners (blue dots), and 12 for broken pipes (green dots) across both floors.

On the first floor (see Fig. 12A), all rooms were observed. Rooms A1, A4, A8, and A11 exhibit a lower potential for condensation as they show no signs of damage. This is likely because these rooms are either not adjacent to technical issues or have proper ventilation. In contrast, rooms A2, A3, and A6 exhibit damage to their building elements. Observations suggest that rooms with technical issues are more likely to experience physical damage.

Room A2 shows yellow stains on the ceiling with lower surface temperatures compared to other areas (spot A2.b). Additionally, some areas on the wood-covered wall in A2 have spots with lower temperatures (spot A2.c), making A2 more prone to further damage. Room A3 displays a medium level of destruction, marked by peeling paint on the walls (spot A3.a). This area is also near a standing air conditioner, which could contribute to condensation and damage. Finally, room A6 has peeling paint and yellow stains on certain wall areas (spot A6.a), likely due to two nearby technical issue spots, including a broken pipe outside the building (see elevation part in Fig. 12A).

On the second floor (see Fig. 12-B), not all rooms have been observed due to similar functions (i.e., prayer areas – B4, B5, B7, B8, B9). In this regard, B1 and B2 are frequently used by the Muslim Youth Community for the event. This makes these rooms often open and shows a propensity for condensation. For example, room B1 shows a peeling paint on the

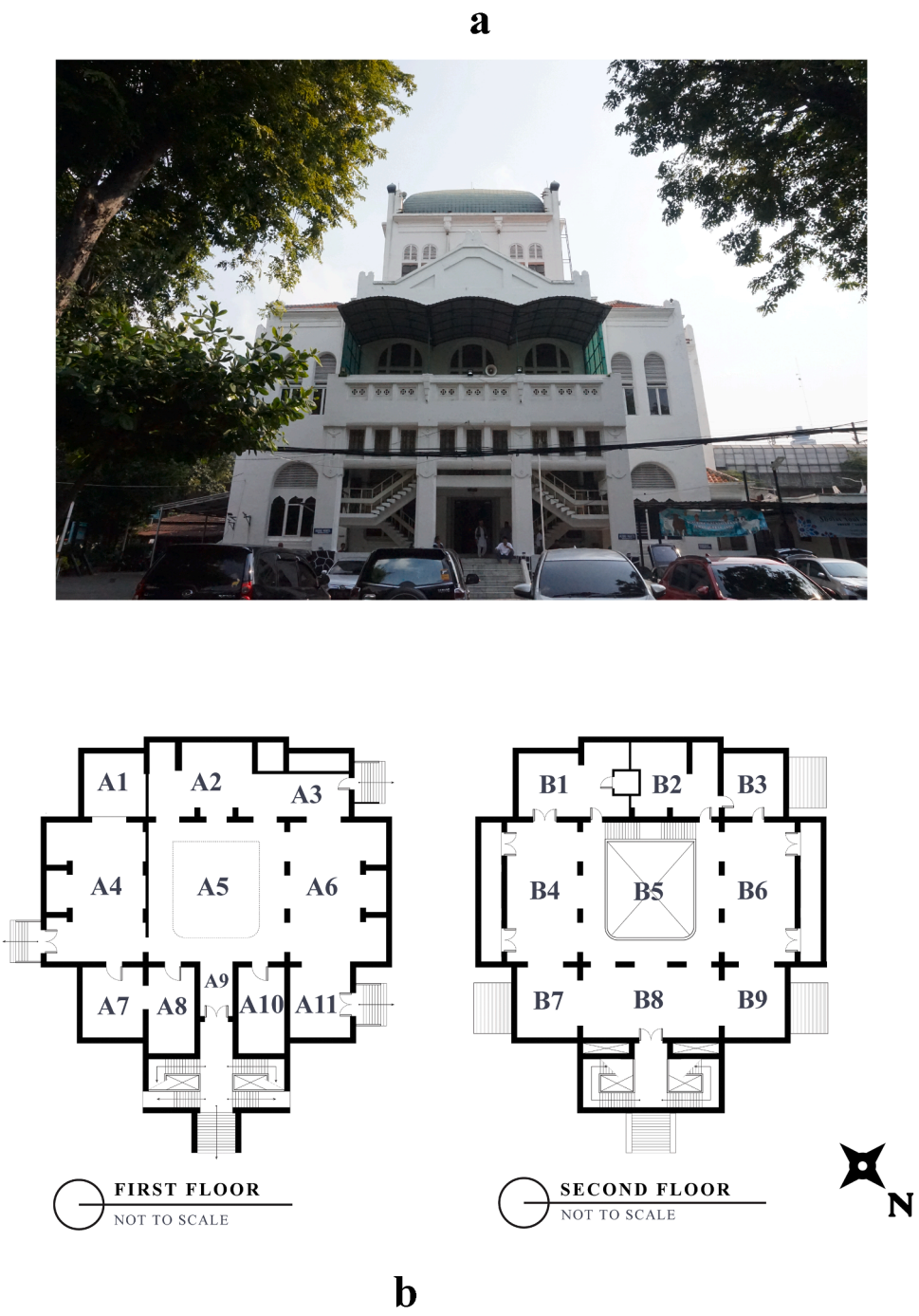

Fig. 10. (a) Cut Meutia Mosque (b) Cut Meutia Mosque Plan [55].

wall, particularly below the indoor unit split AC. This damage likely results from prolonged lack of ventilation and the presence of a water vapor source, specifically the broken indoor unit split AC. Although room B2 also exhibits damage, notably in the ceiling (spot B2.a) due to lack of ventilation, this damage does not come from a water vapor source such as the AC unit.

5.1.2. Environmental performance measurements

By reflecting the presence of water vapor in the room, this study considers relative humidity, dew point temperature, and surface temperature for the environmental performance measurement (see Fig. 13). The horizontal axis represents the time intervals recorded by the data logger, starting from 10:26AM to 1:16PM. The initial investigation results in five rooms (i.e., A2, A3A6, B1, and B2) that are identified as having a potential risk for condensation. These rooms are selected on the basis of relative humidity (RH) threshold value of 40% to detect potential condensation, as previously indicated in Table 1. Furthermore, in order to conduct a comparative analysis with different characteristics, we focus on four different rooms only which are: A2: 51.93 %, A6: 56.12 %, B1: 63.43 %, B2: 57.49 % (see Fig. 13).

From Table 2, it is evident that room A2 has the highest air temperature (33.13 °C). Nevertheless, it shows not only the lowest relative humidity among the rooms observed (51.93 %) and but also the lowest dew-point temperature, namely 20.95 °C. The location of room A2, which is not ventilated and is fully equipped with air conditioning unit, makes it fall into the low-level destruction category. Similar to A2, room A6 is also categorized as the low-level destruction category. According to physical measurements, it was found that old water pipes were

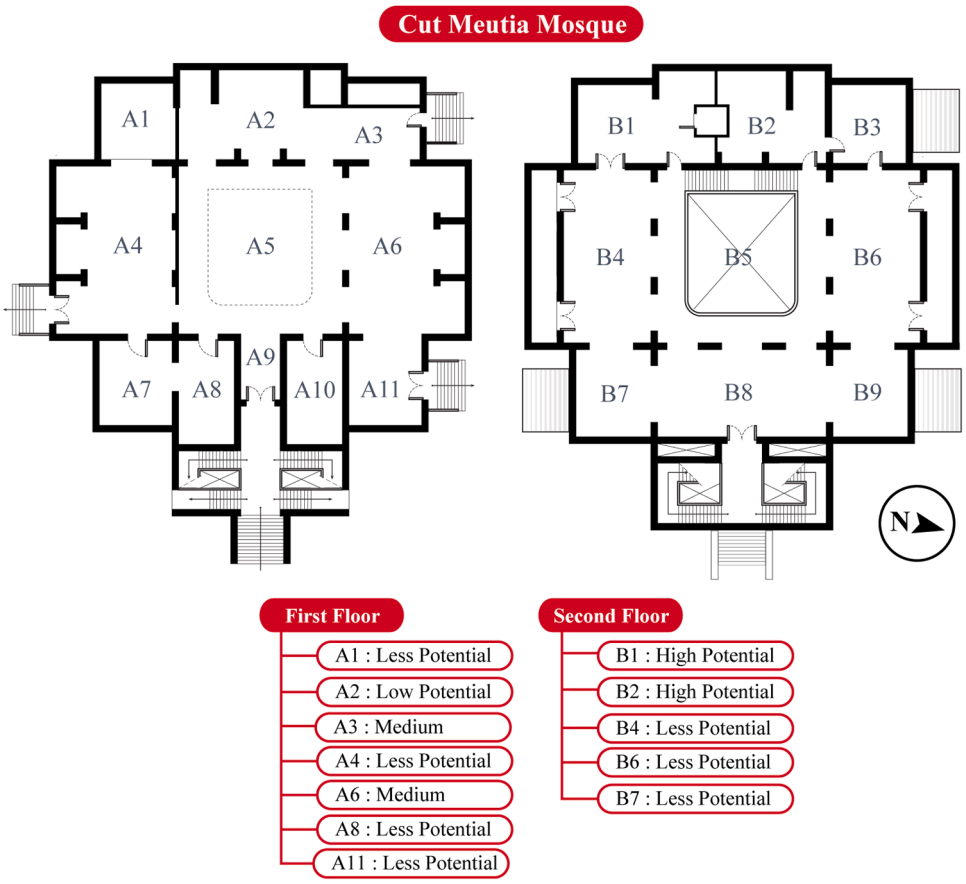

Fig. 11. Mapping of Condensation Risk based on Physical Observation in Cut Meutia Mosque.

attached to the walls and this condition in principle elevates the risk of condensation and structural damage of the room. On the other hand, room B2 and B1 are categorized having high levels of destruction. This is not only due to environmental measurement results but also physical assessment of these rooms that indicate peeling paint, discoloration of the wall, and lack both passive and active ventilation.

Drawing on the above consideration, this study ultimately finds that the selected rooms (i.e., A2, A6, B1, B2) indicate a high potential for condensation based on the results of physical observations that are consistent with environmental parameter measurements.

5.2. Condensation risk area measurement

This section discusses the results of step-by-step condensation risk area measurement. According to the research workflow, for obtaining condensation risk areas, two steps need to be conducted: thermal imagery mapping and correcting BRDF values. Fig. 14 shows the results of both thermal image segmentation and the corrected BRDF dataset, including the condensation risk area measurement. The following subsection explains these results consequently.

5.2.1. Thermal imagery mapping

This section discusses the segmentation of surface temperature in each selected room. This aims to identify specific areas where condensation is likely to occur. Segmentation was conducted with a range of 0.5° to narrow down the investigation process. In this regard, the closer the surface temperature is to the dew point temperature the greater the potential for condensation.

Fig. 14 shows that the surface temperature of most areas is close to the dew point temperature. Color grading helps to pinpoint potential condensation zones more specifically. Additional thermal images depicting different temperature ranges can be found in Appendix 1. In room A2, the dominant surface temperature ranges from 29.5 °C to 30 °C, covering 56.97% of the surface. The dew point in this room is 20.95 °C, resulting in a difference of 9 °C between the surface temperature range and the dew point temperature. Although this difference is quite large, the surface temperature range is the closest value to the dew point temperature.

In room A6, the dominant surface temperature is between 29.5 °C and 30 °C, covering up to 17.23 % of the surface. The dew point in this room is 22.28 °C, resulting in 8 °C difference. This large difference can be attributed to the presence of windows and ventilation, allowing air circulation between rooms.

Room B1 has a dominant surface temperature range of 28 °C to 28.5 °C, covering up to 19.98% of the surface. The dew point temperature in this room is 25.14 °C, with a difference of 3.46 °C. Lastly, B2 has a surface temperature which closest to dew point temperature value namely 29.5 °C and 30 °C, in this room covered up to 3.46 %. In this regard, B1 is the only room with a surface temperature range closest to the dew point temperature. Additionally, the presence of a damaged AC unit causing a peeling paint to suggest significant condensation potential, as this room shows the most signs of damage.

5.2.2. Corrected BRDF dataset

After selecting rooms for condensation risk based on predefined criteria (i.e., relative humidity, surface temperature), the preprocessing of point cloud for geometric and radiometric information is performed to obtain corrected datasets relative to laser reflectance and incident angle. Fig. 13 illustrates BRDF values derived from thermal image segmentation. This process helps visualize the color range of BRDF values in the thermal image segmentation area, indicating the risk of condensation in particular regions.

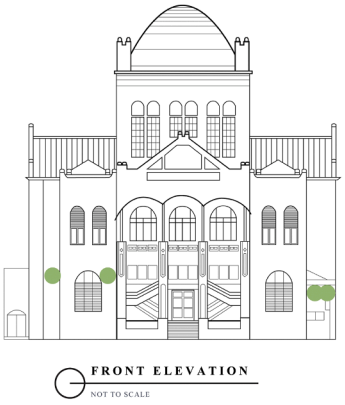

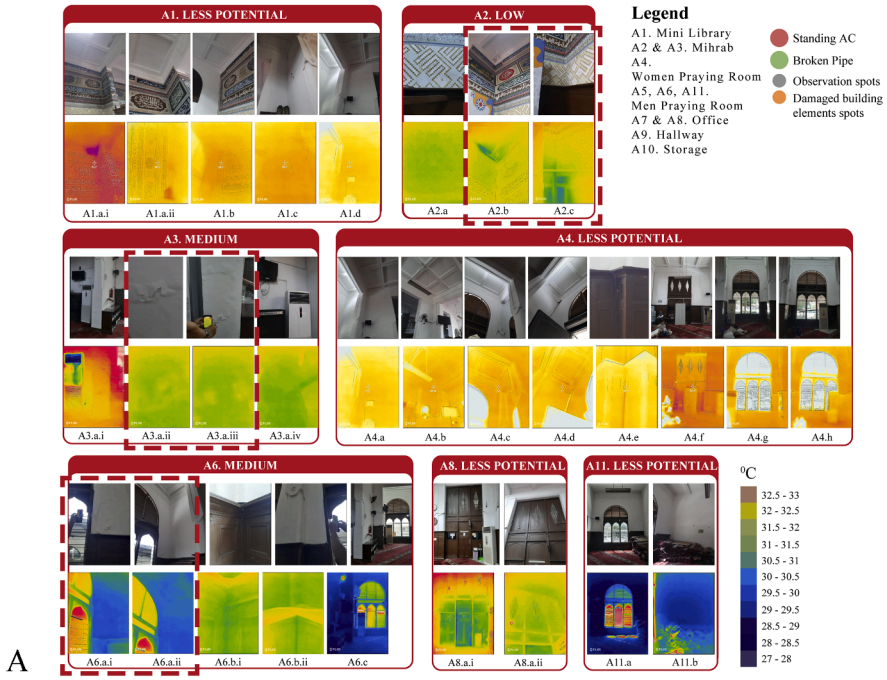

Fig. 12. A. Physical and thermal evaluation of the Cut Meutia Mosque – First floor. 12. B. Physical and thermal evaluation of the Cut Meuta Mosque – Second floor.

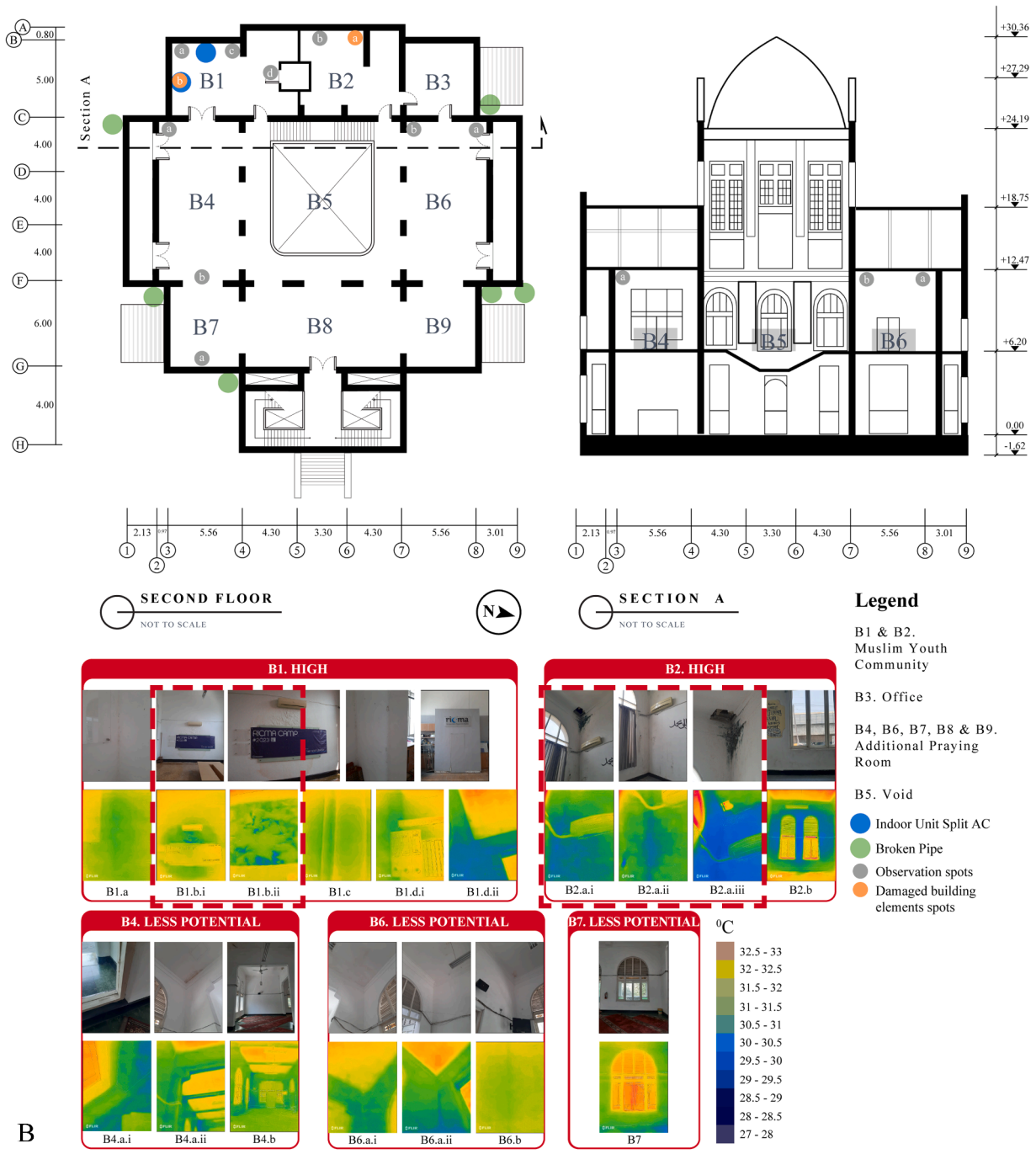

Fig. 12. (*continued*).

In the BRDF color map, blue represents the smallest BRDF values, while red represents the largest one. Principally, smaller BRDF values correspond to fewer specular reflections, which indicates rougher surfaces. When the BRDF value approaches 0, specular reflections disappear, suggesting the presence of substance on the surface. Therefore, areas depicted in blue indicate potential condensation-prone substances. In the selected rooms, several areas displayed blue point clouds, indicating potential condensation risk. In this regard, room A2 showed small BRDF areas on the upper walls and near furniture. Room A6 had small blue BRDF areas in the window frame. Room B1 exhibited small blue BRDF areas in the upper corner of the walls and near the window frame. These results are influenced by environmental measurements, material properties, and luminance availability.

The condensation risk area measurements are obtained by superimposing segmented thermal images and BRDF values in the same viewpoint. The low BRDF range that shows in light blue in segmented A2 covers up the segmentation area by 0.0373 m^2 (Fig. 14). A6's 29.5 to 30 °C segmentation covers up to 0.00581 m^2. B1's have the lowest surface temperature among the rooms, 28 to 28.5 °C covers up to 0.9191 m^2. Lastly, on B2, 29.5 to 30 °C segmentation covers up to 1.257562 m^2. Of the three rooms, the areas with the greatest risk of condensation are B1 and B2, because neither B1 nor B2 have good ventilation. Apart from that, B1 and B2 have sources of water vapor such as leaks from air conditioners and water pipes. A2 and A6 have relatively a small condensation risk area due to room ventilation.

Furthermore, Fig. 15 presents a bar diagram of BRDF values for each room, illustrating the distribution of point cloud data segmented by surface temperature. Each room has a different total number of point

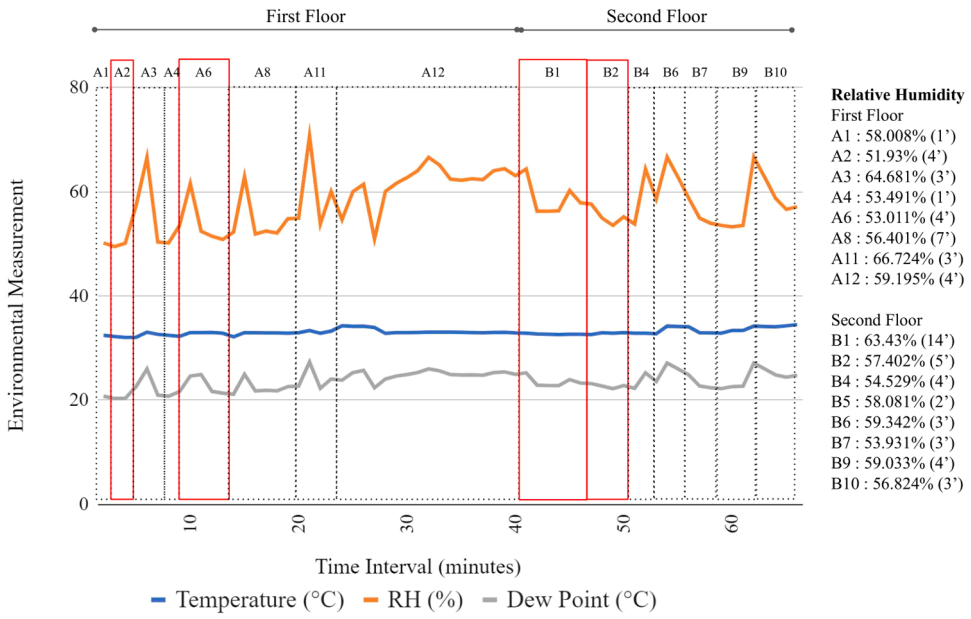

Fig. 13. Environmental parameters evaluation of the Cut Meutia Mosque.

Table 2
Environmental measurement results.

Room	Air temperature (oC)	Relative Humidity %	Dew point (oC) (Td)	Condensation level	Standard
A2	33.13	51.93	20.95	Low level destruction	Condensation happens if:
A6	32.09	56.12	22.28	Low level destruction	RH > 40 %, Ts < Td,
B1	32.99	63.43	25.14	High level destruction	Ts > 25oC (Trecshel [4])
B2	32.65	57.49	23.15	High level destruction	

clouds due to varying segmented surface temperature areas. The minimum value represents the smallest BRDF value, indicating the presence of substances that can cause condensation. Conversely, the maximum value represents the largest BRDF value, suggesting little to no presence of such substances. The mean value refers to the average BRDF, serving as a benchmark to determine the overall trend of BRDF values. The median value provides insights into the skewness of the BRDF dataset. For example, room A2 contains 25.000 point clouds, with a minimum BRDF value of 0.1213, a maximum of 3.2999, a mean of 0.65295, and a median of 0.6978. In general, the BRDF values in A2 tend to approach the minimum borderline, indicating a substantial presence of condensation-causing substances.

On the other hand, room A6 contains around 10.000 point clouds, with a minimum BRDF value of 0.4024, a maximum of 1.4577, a mean of 0.9978, and a median of 0.9894. In contrast, to A2, A6 has fewer BRDF values near the minimum borderline. The mean and median BRDF values in A6 suggest that the majority of point clouds have higher BRDF values, indicating a lesser presence of condensation-causing substances.

As for room B1, it contains 20.000 point clouds, with a minimum BRDF value of 0.8042, a maximum of 1.5357, a mean of 0.9181, and a median of 0.9053. The small difference between the mean and minimum values (0.1139) indicates that most data points have low BRDF values, suggesting a significant potential for condensation. Similar to B1, room B2 also shows a small difference between the mean and minimum values (0.0926), suggesting a potential for condensation. Nevertheless, bar chart shows that B2 has more point clouds that correspond to higher BRDF values that the mean, implying a lower condensation risk compared to B1.

In general, these results validate the potential condensation areas, as the result of superimposing the thermal images with the corrected BRDF values is similar to the BRDF color range.

5.3. Correlation analysis between BRDF values and surface temperature

This section further evaluates the correlation between two variables, BRDF values and surface temperature using Pearson's correlation coefficient.

Before conducting further analysis, the data population sample was determined, with a minimum of 30 paired data values. This is according to the central limit theorem, where 30 values are sufficient for the normal distribution of the paired data of surface temperature and condensation risk area yields from the grid matching process. In this regard, larger areas yield more cells of paired data. For example, room A6 has a condensation risk area of 0.00581 m^2, forming only two cells, which does not meet the minimum requirement of 30 paired values for Pearson's correlation analysis. Therefore, the graph of A6 was removed due to the lack of available data to analyze, whereas the graph of B2 was divided into two parts since the data for each side (left and right) exceeded 30 values.

Fig. 16 further shows that only room A2 that indicates a strong and positive relationship of correlation analysis with an R^2 value of 0.708 (see Fig. 15a). This finding also supports the grid matching, which suggests that room A2 uniquely exhibits a contrasting value pattern and a strong correlation. The lack of consistent patterns in other rooms may be attributed to the fact that only A2 lacks ventilation or apertures for natural light penetration, making it more prone to higher humidity levels.

6. Implications and discussions

6.1. Implications

The study's findings make a significant contribution to the preservation of heritage buildings by offering a reliable method for early detection of condensation risks. This approach supports architects and conservators in making informed decisions to protect and maintain these structures. Moreover, the study highlights gaps in current Indonesian

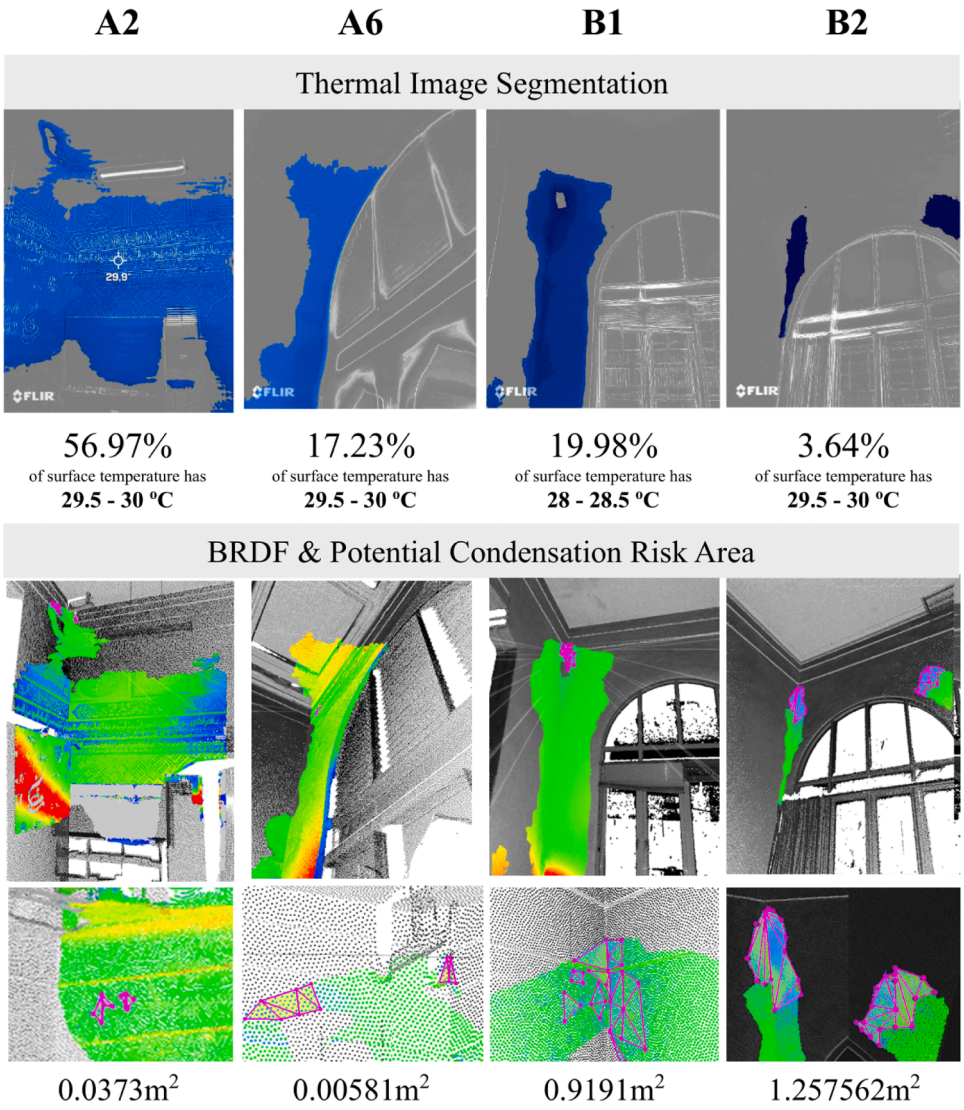

Fig. 14. Thermal Image Segmentation results, BRDF and Potential Condensation Risk Area.

regulations regarding moisture presence and condensation risk detection in heritage buildings. It suggests that incorporating physical, biological, and chemical parameters comprehensively could improve preservation standards and guidelines. Currently, Indonesian Law Number 11 of 2010, Chapter VII, states that preservation should be accountable academically, technically, and administratively. We recommend adding a provision to the law that emphasizes the importance of environmental measurements in preservation techniques, to raise awareness of the role of physical, biological, and chemical parameters in preserving heritage buildings. The findings of this research, which include preliminary surveys, condensation risk measurements, and the correlation analysis between BRDF values and surface temperature, align with the principles of various green building certification systems, such as GBI, BREEAM, LEED, DGNB, and Greenship. These systems emphasize the importance of indoor environmental quality, energy efficiency, and proper ventilation to prevent issues like condensation, which can affect building longevity and occupant comfort. For instance, the study's identification of rooms with poor ventilation and the impact of HVAC systems aligns with BREEAM and LEED's focus on managing indoor air quality and thermal comfort. The measurement of relative humidity and surface temperature reflects GBI's focus on maintaining optimal conditions for building materials to prevent degradation. Additionally, DGNB's holistic approach to building quality aligns with the study's analysis of technical issues, such as broken pipes and faulty air conditioners, which contribute to condensation. Insights into the detrimental effects of high humidity levels in rooms further support the goals of Greenship, which prioritizes sustainable building practices in tropical climates like Indonesia's. Overall, the study underscores the importance of aligning building conservation efforts with the sustainability criteria set by green building certification systems to ensure a balanced and resilient indoor environment.

6.2. *Discussion*

In general, the results of this study demonstrate that the proposed method enhances the detection of condensation risks in heritage buildings by utilizing BRDF values and surface temperature. Specifically, the integration of 3D laser scanning and thermal imaging techniques aids architects and conservators in preventing leaks or damage in heritage buildings and complements empirical approaches for detecting condensation risks, such as those by Lerones et al. [11] and Ham & Golpavar-Fard (2014). Additionally, Halim et al. [56] comprehensively investigated dampness in historic buildings using visual inspections and both non-destructive and destructive methods, such as a protimeter and drying techniques. Although thorough, their analysis involved tools that made contact with building materials, potentially causing damage.

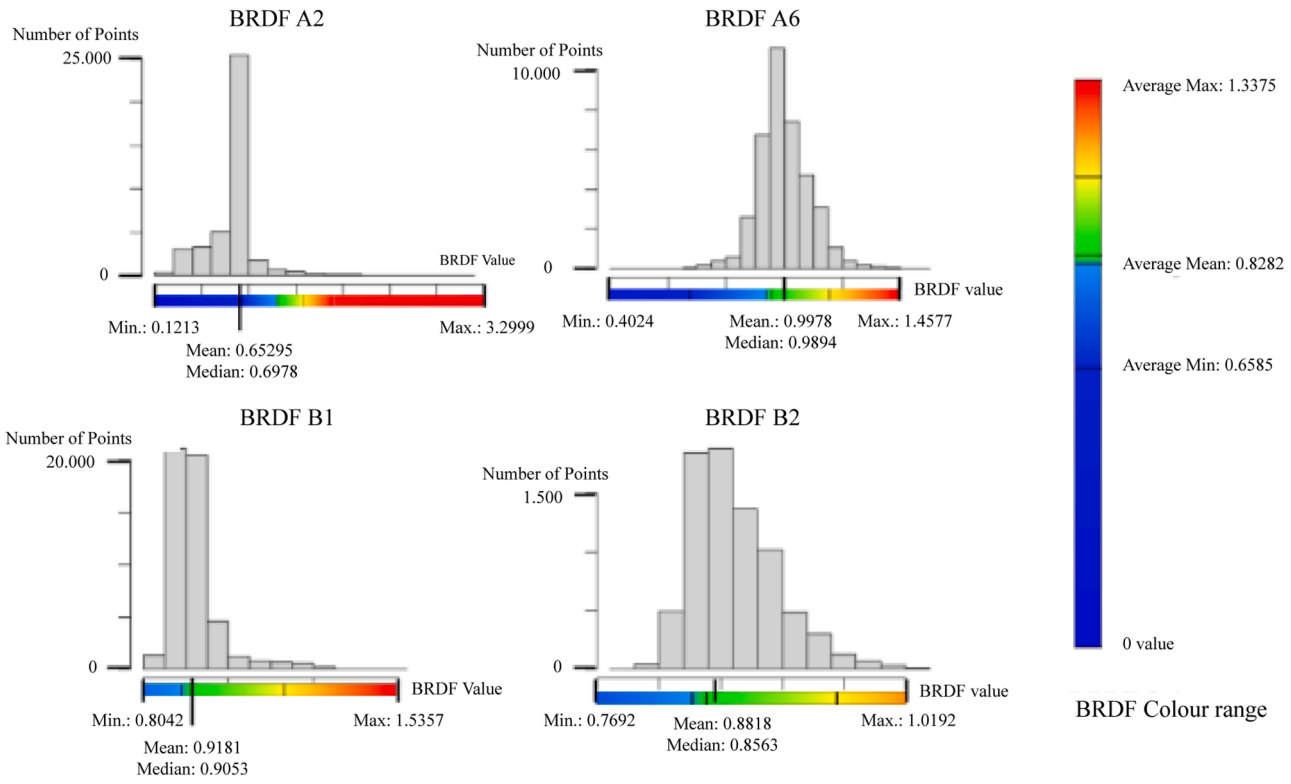

Fig. 15. BRDF colour range based in average mean of BRDF value of each selected room.

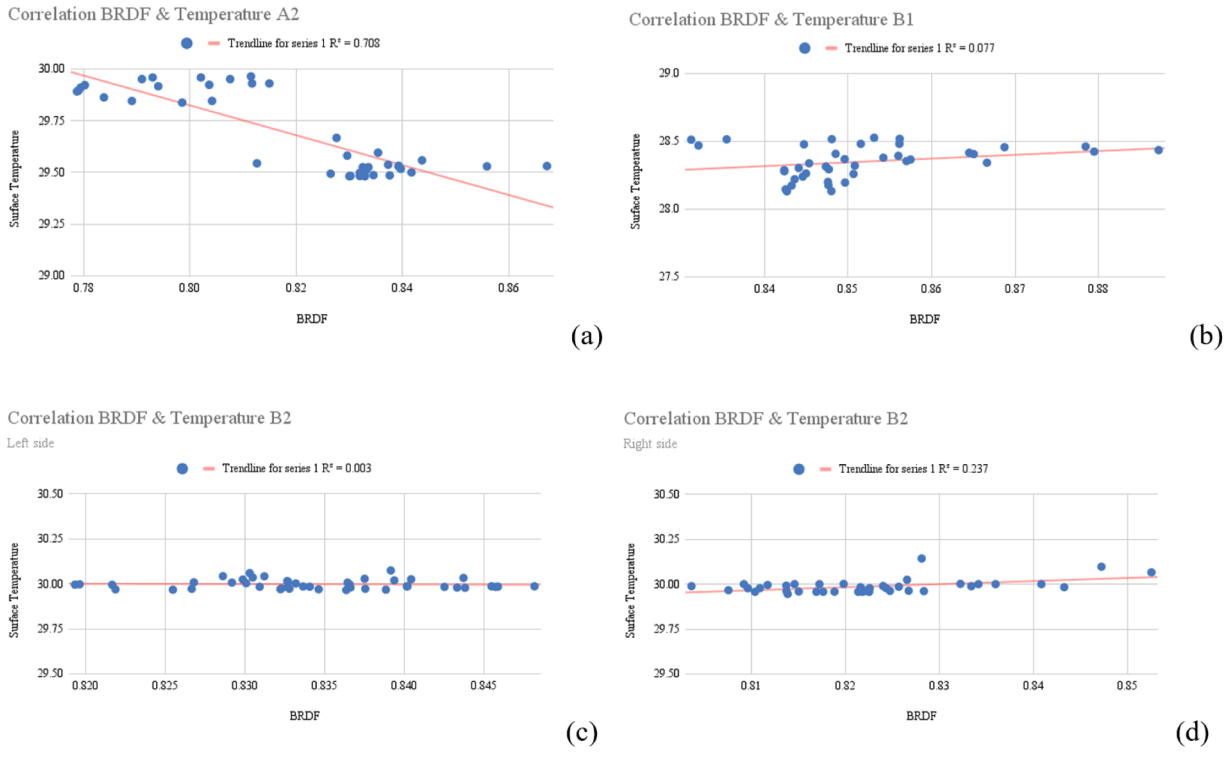

Fig. 16. Pearson correlation between BRDF and Surface Temperature.

Therefore, methods that avoid direct contact while detecting condensation should be further developed. Other tools, such as those that emit infrared and radar signals, have been explored for detecting moisture in materials, including Infrared Thermography (IT), Unilateral NMR, Contactless Acoustic Imaging (AI), Acoustic Tomography (AT), and LIF Measurement [32]. Parameters such as surface temperature, water infiltration levels, efflorescence, sonic velocity, and acoustic absorption percentage are effective in detecting condensation and moisture in building materials. Despite the appeal of this multidisciplinary approach, these methods require careful calibration and accuracy

adjustments for diverse contexts. Similar tools, like the Terrestrial Laser Scanner, microwave, and radar, have been used to monitor moisture levels in stone masonry, particularly in a sandstone tower and granite wall [31]. Non-destructive techniques such as radar and microwave sensors have proven effective in detecting moisture variation and assessing water penetration through masonry joints, offering a reliable alternative for moisture monitoring without physical intrusion [31]. These methods are particularly sensitive to changes in surface and near-surface moisture, making them suitable for tracking the progression of moisture levels over time.

Although standards and regulations regarding moisture presence and condensation risk are outlined in the Indonesian Law on Heritage Buildings (No. 11 of 2010) [57] and the Technical Module for Preservation from the Ministry of Education, Culture, Research, and Technology [58], neither the law nor the module comprehensively specifies physical, biological, or chemical parameters for detecting condensation risks. This study, therefore, provides significant contributions to detecting condensation risks, especially within the context of heritage buildings in Indonesia. Our proposed method enables architects and conservators to identify and assess the microclimatic influence on existing building surfaces early, before physical damage occurs.

7. Conclusion

This study has developed a computational workflow for detecting potential condensation risks in heritage building surfaces based on technological integration between 3d scanning and thermal imaging techniques. More specifically, this study investigates geometric and radiometric properties of point cloud data in order to calculate BRDF, emissivity values, and albedo.

Key findings of this study can be summarized as follows:

- This study identifies that the selected rooms (A2, A6, B1, B2) have a significant potential for condensation, as indicated by physical observations that match the environmental parameter measurements. The analysis shows that Room B2 has the highest area at risk for condensation, measuring 1.257562 m^2, while the risk areas for the other rooms are 0.0373 m^2 (Room A2), 0.00581 m^2 (Room A6), and 0.9191 m^2 (Room B1). Additionally, the Pearson correlation analysis revealed that only Room A2 exhibited a strong correlation between surface temperature and BRDF when identifying condensation. This could be attributed to the lack of ventilation or openings for natural light in Room A2, making it more susceptible to increased humidity levels.
- Condensation risk factors and room-specific observations to determine early condensation risk. This study identified several factors contributing to condensation risk, such as technical issues, ventilation and environmental conditions. From those condensation risk factors, it possible to develop the level of condensation risk such as high, medium, low and less potential. For example, Rooms B1 and B2 were identified as having the highest risk for condensation due to technical issues and lack of ventilation. Moreover, Rooms A2 and A6 showed moderate risk, with some condensation-prone areas identified through BRDF values and thermal imagery. Meanwhile, rooms with proper ventilation and fewer technical issues exhibited lower risk for condensation.
- Conceptual integration between BRDF and surface temperature. This study confirms a strong correlation for both aspects when it comes to the condensation detection. In this regard, BRDF calculates specular reflection, indicating that surfaces with low BRDF values exhibit specular reflection materials. This specular reflection can then be assumed to signify the presence of water vapor in the initial phase of condensation. On the other hand, surface temperature which positively correlated with condensation area has been validated as a parameter for detecting condensation on a surface. Our findings demonstrate further that although BRDF and surface temperature share similarities for identifying the surface characteristics of condensation risks, their correlation still depends on specific conditions of the room.

Notwithstanding the constraints of our investigation, a few points need further consideration. For example, the collected surface temperature of the wall from the data logger currently detects temperature only in imagery format and this makes it difficult to produce precise synchronization for geometric point clouds. In addition, photogrammetry techniques may provide great potential to our methods by using orthothermal images and using reference points such as ice cubes. Furthermore, to enhance the robustness of the analysis, environmental measurements should be collected at various times throughout the day and across different seasons. This approach enables a comprehensive assessment of how condensation risks vary in response to changing climatic condition.

CRediT authorship contribution statement

Miktha Farid Alkadri: Writing – review & editing, Supervision, Methodology, Funding acquisition, Conceptualization. **Yuliana Yuliana:** Writing – original draft, Visualization, Project administration, Methodology, Investigation, Formal analysis. **Muhammad Rafif Cahyadi Agung:** Investigation, Methodology, Writing – original draft, Visualization, Software. **Muhammad Arif Rahman:** Writing – original draft, Visualization, Software, Methodology, Investigation. **Carola Hein:** Writing – review & editing, Supervision, Conceptualization.

Declaration of competing interest

The authors declare that they have no known competing financial interests or personal relationships that could have appeared to influence the work reported in this paper.

Acknowledgements

This work was supported by the Directorate of Research and Development (DRPM) University of Indonesia under Hibah PUTI 2023 (Grant no. NKB-526/UN2.RST/HKP.05.00/2023) awarded to Dr. Miktha Farid Alkadri, S.Ars., M.Ars

Supplementary materials

Supplementary material associated with this article can be found, in the online version, at doi:10.1016/j.rineng.2024.103292.

Data availability

Data will be made available on request.

References

[1] RICS, Investigation of Moisture and its Effects in Traditional Buildings, 2019 [Online], Available at, https://www.heritage-house.org/documents/RICS-Historic-England-joint-methodology.pdf.
[2] E. Sesana, et al., Climate change impacts on cultural heritage: a literature review, WIREs Clim. Change 12 (2021) 1–29, e710.
[3] D. Tifada, A. Winardi, Gudang Timur Batavia: bangunan Cagar Budaya di Jakarta yang Tak Terpelihara, 2022 [Online], Available at, https://voi.id/memori/176598/gudang-timur-batavia-bangunan-cagar-budaya-di-jakarta-yang-tak-terpelihara (Accessed 15 September 2023).
[4] H. Trecshel, Moisture Analysis and Condensation Control in Building Envelopes, ASTM, 2003. Volume 40, https://www.astm.org/stp10936s.html.
[5] L. Thomas, Moisture Analysis Techniques, 2018 [Online], Available at, https://www.news-medical.net/life-sciences/Moisture-Analysis-Techniques.aspx (Accessed 19 September 2023).
[6] C. Ranwell, Detecting the Difference Between Rising Damp Vs. Condensation, 2023 [Online]Available at, https://blog.protimeter.com/blog/rising-damp-vs.-condensation (Accessed 20 December 2023).

[7] EPA, Moisture Control Guidance for Building Design, Construction and Maintenance, 2013 [Online] Available at, https://www.epa.gov/sites/default/files/2014-08/documents/moisture-control.pdf (Accessed 27 August 2023).
[8] P. Barone, C. Ferrara, Non-invasive moisture detection for the preservation of cultural heritage, Heritage 1 (1) (2018) 163–170.
[9] M. Saban, et al., Sensing wood moisture in heritage and wooden buildings: a new sensing unit with an integrated LoRa-based monitoring system, IEEE Internet Things J. 9 (24) (2022) 25409–25423.
[10] M. Muradov, et al., Non-destructive system for in-wall moisture assessment of cultural heritage buildings, Measurement 203 (2022) 1–17.
[11] P. Lerones, et al., Moisture detection in heritage buildings by 3D laser scanning, Stud. Conserv. 61 (1) (2016) 46–54.
[12] Mettler Toledo, 2023. Guide to Moisture Analysis. [Online], Available at: https://www.mt.com/us/en/home/library/guides/laboratory-weighing/guide-to-moisture-analysis.html, (Accessed 15 November 2023).
[13] A. Anca-Couce, et al., Characterization and condensation behaviour of gravimetric tars produced during spruce torrefaction, J. Analyt. Appl. Pyrol. 119 (2016) 173–179.
[14] P. Dash, et al., Detecting moisture in building materials and commercial food adducts by 2-hydroxy-naphthaldehyde derived chromo-fluorogenic chemosensor, J. Fluoresc. 23 (5) (2024) 1–13.
[15] R. Richter, J. Döllner, Concepts and techniques for integration, analysis and visualization of massive 3D point clouds, Comput. Environ. Urban. Syst. 45 (2014) 114–124.
[16] G. Rocha, L. Mateus, J. Fernandez, V. Ferreira, A Scan-to-BIM methodology applied to heritage buildings, Heritage 3 (1) (2020) 47–67.
[17] M.F. Alkadri, et al., Investigating surface fractures and materials behavior of cultural heritage buildings based on the attribute information of point clouds stored in the TLS dataset, Remote Sens. 14 (2) (2022) 210.
[18] Bonora, A., Fabbri, K. & Pretelli, M., 2021. Historic indoor microclimate, the role of HVAC in heritage buildings' restoration: the case of the Palace of Venaria Reale. s. l., J.Phys.
[19] E. Lucchi, Energy performance indicators for Air-conditioned museums in tropical climates, Buildings 14 (2301) (2024).
[20] D. White, LIDAR, point clouds, and their archaelogical applications. Mapping Archaeological Landscapes from Space, Springer-Verlag, New York, 2013, pp. 86–173.
[21] J. Otepka, et al., Georeferenced point clouds: a survey of features and point cloud management, ISPRS Int. J. Geo-Inf. 2 (4) (2013), 2038-1065.
[22] M.F. Alkadri, An integrated approach to subtractive solar envelopes based on attribute information from point cloud data, Renew. Sustain. Energy Rev. 123 (2020) 1–19.
[23] I. Kobayashi, Y. Fujita, H. Sugihara, K. Yamamoto, Attribute analysis of point cloud data with color information, J. Japan Soc. Civil Eng. 67 (2) (2011) 95–102.
[24] Y. Fujita, Y. Hoshino, S. Ogata, I. Kobayashi, Attribute assignment to point cloud data and its usage, Glob. J. Comput. Sci. Technol. 15 (2) (2015) 11–18.
[25] Y. Fujita, I. Kobayashi, Y. Hoshino, W. Chanseawrassamee, Development of attribute-assign-editor for road surface point cloud data, IACSIT Int. J. Eng. Technol. 8 (3) (2016) 170–176.
[26] Sidiropoulou-Velidou, D., Georgopoulos, A. & Lerma, J., 2012. Exploitation of thermal imagery for the detection of pathologies in monuments. Limassol, s.n.
[27] Salehi, V. & Wang, S., 2017. Using Point Cloud Technology For Process Simulation in the Context of Digital Factory Based On a System Engineering Integrated Approach. Vancouver, s.n.
[28] Zhan, Q., Liang, Y. & Xiao, Y., 2009. Color-based segmentaion of point clouds. France, s.n.
[29] T. Voegtle, I. Schwab, T. Landes, Influence of different materials on the measurements of a terrestrial laser scanner (TLS), Int. Arch. Photogramm, Remote Sens. Spat. Inf. Sci 37 (5) (2008) 1061–1066.
[30] H. Laasch, T. Medic, A. Wieser, Towards assessing sandstone surface moisture and degradation level from radiometrically corrected TLS intensity data, in: Cairo, ISPRS Annals of the Photogrammetry, Remote Sensing and Spatial Information Sciences, 2023.
[31] S.A. Orr, et al., Moisture monitoring of stone masonry: a comparison of microwave and radar on a granite wall and a sandstone tower, J. Cult. Herit. 41 (2020) 61–73.
[32] N. Proietti, et al., Moisture damage in ancient masonry: a multidisciplinary approach for in situ diagnostics, Minerals 11 (4) (2021).
[33] M. Marcelić, R. Malarić, System For Early Condensation Detection and Prevention in Residential Buildings, IEEE, Opatija, 2017, pp. 162–165.
[34] N. Brown, R. Laing, J. Scott, The doocots of Aberdeenshire: an application of 3D scanning technology in the built heritage, J. Build.Apprais. 4 (2009) 247–254.
[35] F.R.d. Alfano, B.I. Palella, G. Riccio, Moisture in historical buildings from causes to the application of specific diagnostic methodologies, J. Cult. Herit. 61 (2023) 150–159.
[36] NASA, 2017. What is Albedo?. [Online], Available at: https://mynasadata.larc.nasa.gov/mini-lessonactivity/what-albedo, (Accessed 12 September 2023).
[37] F.E. Nicodemus, et al., Geometrical Considerations and Nomenclature For Reflectance, United States: Jones and Bartlett Publishers, Inc., Radiometry, 1992, pp. 94–145.
[38] Y. Zou, et al., Developmental trends in the application and measurement of the bidirectional reflection distribution function, Sensors 22 (5) (2022) 1739.
[39] J. Shell, Bidirectional reflectance: an overview with remote sensing applications & measurement recommendations, Environ. Sc. (2004) 1–76.
[40] Montes, R. & Urena, C., 2012. An Overview of BRDF Models. Technical Report LSI, Volume 001, pp. 1–26.
[41] C. Wynn, An introduction to BRDF-based lighting, Physica D (2000) 105–112.
[42] F. Guo, et al., A modified BRDF model based on cauchy-lorentz distribution theory for metal and coating materials, Photonics. 10 (7) (2023) 773.
[43] M. Pharr, W. Jakob, G. Humphreys, Physically based rendering: from theory to implementation. Physically Based Rendering, 2018 s.l.:pbr-book.org, p. 1.
[44] B.T. Phong, Illumination for computer generated pictures, Commun. ACM 18 (6) (1975) 311–317.
[45] Shaders Monthly, Blinn Phong Shading: Theory and Implementation, 2022 s.l.:GSN Composer.
[46] A. Angstrom, The Albedo of Various Surfaces of Ground, Geografiska Annaler, 1925, pp. 323–342.
[47] J.B. Nielsen, et al., A Variational Study On BRDF Reconstruction in a Structured Light Scanner, IEEE, Venice, 2017, pp. 143–152.
[48] ISO, ISO 22185-1:2021 Diagnosing Moisture Damage in Buildings and Implementing Countermeasures, 2021 [Online] Available at, https://www.iso.org/standard/72824.html [Accessed 23 August 2023].
[49] U. Haverinen, et al., Characteristics of moisture damage in houses and their association with self-reported symptoms of the occupants, Indoor Built Environ. 10 (2) (2001) 83–94.
[50] J. Zhang, C.C. Chan, H.H. Kwok, C.J. Cheng, Multi-indicator adaptive HVAC control system for low-energy indoor air quality management of heritage building preservation, Build. Environ. 246 (2023).
[51] C. Lerma, et al., Evaluation of hygrothermal behaviour in heritage buildings through sensors, CFD modelling and IRT, Sensors 21 (566) (2021) 1–19.
[52] K. Tan, X. Cheng, Surface reflectance retrieval from the intensity data of a terrestrial laser scanner, J. Opt. Soc. Am. A 33 (4) (2016) 771–778.
[53] J.F. Blinn, Models of Light Reflection For Computer Synthesized Pictures, Association for Computing Machinery, San Jose, 1977, pp. 192-198.
[54] Masjid Cut Meutia, n.d. Sejarah Masjid Cut Meutia. [Online], Available at: https://masjidcutmeutia.com/sejarah/, (Accessed 13 July 2023).
[55] Y.A. Waspodo, Gedung Bouwploeg (Masjid Cut Mutia), Menteng Tinjauan Perkembangan Bentuk Arsitektural, Universitas Indonesia, Depok, 2009.
[56] A.-H. Halim, S.N. Harun, Y. Hamid, Diagnosis of dampness in conservation of historic building, J. Design + Built (2012) 1–14.
[57] Kebudayaan Kemdikbud, Cagar Budaya, Kemdikbud, Jakarta, 2010.
[58] D. Suhardi, H. Farid, G.S. Utami, F. Arda, Modul Pelatihan Teknis Pemugaran Cagar Budaya untuk Juru Pelestari Cagar Budaya, 2018 [Online], Available at, https://repositori.kemdikbud.go.id/17911/ (Accessed 1 June 2024).